Articles in PresS. Am J Physiol Lung Cell Mol Physiol (August 3, 2017). doi:10.1152/ajplung.00185.2017

Platelet-derived growth factor receptor-alpha (PDGFRα) and Ras-related C3 botulinum toxin substrate-1 (Rac1) regulate mechano-responsiveness of lung fibroblasts

Stephen E. McGowan and Diann M. McCoy

Department of Veterans Affairs Research Service and Department of Internal Medicine, University of Iowa Carver College of Medicine, Iowa City, Iowa USA

Running title: Regulation of mechano-responsiveness in lung fibroblasts

Address correspondence to

Stephen McGowan M.D.
Division of Pulmonary, Critical Care, and Occupational Medicine
C33B GH
Department of Internal Medicine
University of Iowa Hospitals and Clinics
200 Hawkins Dr.
Iowa City, Iowa 52242
stephen-mcgowan@uiowa.edu
Phone 319-356-1013

Abstract

Platelet-derived growth factor (PDGF)-A, which only signals through PDGF-receptor-alpha (PDGFRα) is required for secondary alveolar septal formation. Although PDGFRα distinguishes mesenchymal progenitor cells during the saccular stage, PDGFRα-expressing alveolar cells persist through adulthood. PDGF-A sustains proliferation, limits apoptosis, and maintains alpha-smooth muscle actin (αSMA) containing alveolar cells, which congregate at the alveolar entry ring at postnatal day (P)12. PDGFRα-expressing, αSMA-containing, alveolar cells re-distribute in the elongating septum, suggesting that they migrate to the alveolar entry rings where mechanical tension is higher. We hypothesized that PDGFRα and Ras-related C3 botulinum toxin substrate 1(Rac1) are required for mechanosensitive myofibroblast migration. Spreading of PDGFRα-deficient lung fibroblasts was insensitive to increased rigidity, and their migration was not reduced by Rac1-guanine exchange factor (GEF)-inhibition. PDGFRα-expressing fibroblasts migrated towards stiffer regions within 2-dimensional substrates by increasing migrational persistence (durotaxis). Using a Förster resonance energy transfer (FRET) biosensor for Rac1-GTP, we observed that PDGFRα was required for fibroblast Rac1-responsiveness to stiffness within a 3-dimensional collagen substrate, which by itself increased Rac1-FRET. Rho-GTPase stabilized whereas Rac1-GTPase increased the turnover of focal adhesions. Under conditions which increased Rac1-GTP, PDGFRα signaled through both phosphoinositide-3-kiase (PIK) or Src to engage the Rac1 guanine-exchange factors (GEF)s dedicator of cytokinesis-1 (Dock180) and p21-activated-kinase interacting exchange factor-β (βPIX). In cooperation with collagen fibers, these signaling pathways may guide fibroblasts toward the more rigid alveolar entry ring during secondary septation. Because emphysema and interstitial fibrosis disrupt the parenchymal mechanical continuum, understanding how mechanical factors regulate fibroblast migration could elicit strategies for alveolar repair and regeneration.

Introduction

Secondary alveolar septation, which in mice exclusively and in humans primarily occurs after birth, geometrically increases gas-exchange surface area (7). Secondary septa arise from primary septal crests, in locations where α-smooth muscle actin-containing interstitial mesenchymal cells (myofibroblasts), lie adjacent to elastic fibers, which eventually assemble into a continuous network. Elastic fiber density varies along the network and is highest at septal tips and bends, where myofibroblasts congregate and contribute to locally elevated mechanical tension (41) (47). During secondary septation, collagen gene expression peaks ahead of elastin and before alveolar myofibroblasts are most abundant. Discontinuous collagen fibers first appear in the termini and then within the walls of expanding saccules (58), becoming more continuous, interweaving with elastic fibers to form cables, and congregating at the alveolar entry rings, This progressive contiguity is consistent with dual production of collagen and elastin by fibroblasts. Studies performed during alveolar development (9), regeneration after pneumonectomy (23) and repair following injury induced by bleomycin (63) or elastase (46), have all established that alpha smooth muscle actin (αSMA)-containing alveolar myofibroblasts deposit both collagen and elastic fibers. In adult lungs, elastic fibers form the core of stress-bearing cables, suggesting that the collagen network underwent remodeling and relocation (1).

In destructive parenchymal lung diseases, including bronchopulmonary dysplasia, emphysema and pulmonary fibrosis, interstitial fibroblasts fail to maintain the normal alveolar architecture and the load-bearing elastic network. Abnormal myofibroblasts are central to these defects. In pulmonary fibrosis, myofibroblast apoptosis is reduced and excessive collagen thickens the alveolar walls and promotes alveolar collapse (24). In emphysema, myofibroblast apoptosis is increased, leaving a larger proportion of interstitial fibroblasts, which are not myofibroblasts (49). Increased myofibroblast signaling through Rho-GTPase contributes to pulmonary fibrosis (65), but less is known about mechanosensitive Rho-family GTPase-signaling during emphysematous distortion of the continuum of interstitial collagen and elastic fibers.

Although more attention has been paid to elastic fibers, collagen fibers are also altered in

emphysema. Collagen degradation products are increased in humans with COPD: both urine pyridinolines (52) and serum collagen endo-peptides (51). Circulating procollagen peptides are elevated following COPD exacerbations, consistent with active collagen synthesis (51). When administered intratracheally to mice, porcine pancreatic elastase increases, rather than decreases collagen (42) (14), particularly in regions of emphysema. Other studies suggest that a non-uniform distribution of collagen produces mechanical forces, which propagate emphysema after inflammation abates (17). It remains unclear how anatomical and mechanical distortion impact the ability of fibroblasts to restore the alveolar architecture.

Signaling by PDGF-AA (PDGF-A) through PDGFRα is required to establish and maintain the myofibroblast precursor population (33). During secondary septation, PDGFRα-expressing myofibroblasts progressively congregate at the alveolar entry ring, which forms the septal tip in planar sections. This distal relocation likely involves cell migration, but it remains unclear what drives migration. Although PDGF-A stimulates migration, a distally increasing septal chemotactic gradient has not been demonstrated. The Rho-GTPase family member Rac1 is essential for mesenchymal cell migration and its abundance in the active GTP-bound state is controlled by (a) guanine-exchange factor (GEF)s which promote and (b) GTPase-activating proteins (GAP)s, which reduce GTP-binding; and by (c) guanine nucleotide dissociation inhibitors (GDI)s which sequester Rac1 in the cytoplasm.

We hypothesized that PDGFRα and Rac1 are required for mechanosensitive myofibroblast migration. To address this hypothesis, we have studied mechanosensitive spreading and migration by fibroblasts either expressing or lacking PDGFRα. Cell migration along an axis of increasing substrate stiffness (durotaxis) was studied using PDGFRα-expressing mouse LF. Figure 1A schematically depicts how PDGFRα signals to Rac1 at the leading edge of polarized, migrating fibroblasts. Signaling through PDGFRα and Rac1 enhanced migration, which was reduced when fibroblasts lacked PDGFRα.

Materials and Methods

Materials

Reagents: LY-294002 –hydrochloride #L9908, fibronectin adhesion promoting peptide, #F3667,

SigmaAldrich, St. Louis MO; NSC23766, catalog #1261; Y27632, #1254; U73122, #1268; Tocris, Minneapolis, MN; Lipofectamine 2000, Hams F12, OptiMEM medium, FluoroBrite™ DMEM medium, Sulfo-SANPAH, #22589 and ToPro-3 ThermoFisher, Waltham, MA; human rPDGF-A, 221AA, human rVitronectin #2308VN, R&D Systems, Minneapolis, MN; Acti-stain A488 phalloidin, #PHDG1 Cytoskeleton Inc. Denver, CO;. Easy Coat activated Softview™ hydrogels 1, 8 and 25 kPa, Matrigen, Brea, CA; Nusil gel 8100, Nusil Technology, Carpinteria, CA; Sylgard 184, Dow Corning, Midland, MI;. *Antibodies*: anti-talin, goat-anti human C-terminus, sc-7534, SantaCruz Biotech. Dallas, TX; anti-phospho paxillin (Tyr118), #2541S, Cell Signaling Technology, Danvers, MA; anti-p130Cas (BCAR1), goat polyclonal, #OAEB03174, and anti-β-PIX (ARHGEF1) rabbit polyclonal, #OASG05888, AVIVA Systems, San Diego, CA; anti-ELMO1 rabbit polyclonal #PA5-28406, Thermo Fisher; anti-Paxillin, sheep polyclonal, #AF4259, R&D Systems, Minneapolis, MN. Plasmids and vectors: mCerulean N1, #27795, mVenus N1, #27793, Addgene, Cambridge, MA; Modification V2 Rac1 WT FRET (Förster resonance energy transfer) biosensor: mCerulean donor and mVenus acceptor (Louis Hodgson, Albert Einstein University, New York, NY) (38). The biosensor was cloned into the pacAd5CMVmcspA shuttle vector and incorporated into Adenovirus 5, University of Iowa Viral Vector Core, Iowa City, IA.

Mice: Mice with a targeted deletion of LoxP- *pdgfrα* have been described (35). The DNA coding Cre-recombinase was inserted into exon -1 of *transgelin* (*tagln*, TG) and mediates Cre-recombination postnatally but not in the embryo (62). Transgelin is expressed in pulmonary myofibroblasts, pericytes and smooth muscle cells. The genotype for mice with the conditional PDGFRα-gene deletion was TGCre+/-;PDGFRαFlox/Flox (PDGFRαF/F). Littermate controls whose genotype was TGCre+/-;PDGFRαF/- were phenotypically indistinguishable from wildtype mice (TGCre-/-, no LoxP flanked alleles). Mice bearing the PDGFRα-GFP construct have been described (21). Production of GFP, which bears a nuclear localization signal, is under the control of the endogenous *pdgfrα* promoter. GFP expression in the PDGFRα-GFP mice spatially and temporally recapitulates endogenous *pdgf-rα* expression (15). The heterozygous mice used in this study carried one *pdgfrα*-GFP allele (which does

not encode for active PDGFRα) and one functional *pdgfrα* allele and are phenotypically identical to wildtype (GFP^-) mice. Littermate controls did not bear a PDGFRα-GFP allele. Protocols for animal use were approved by the Iowa City Veterans Affairs Medical Center animal use committee.

Methods

Isolation of primary mouse fibroblasts Lung fibroblasts (LF) were isolated on P8from TGCre+/-;PDGFRαF/F, double heterozygous littermates controls (TGC+/-;PDGFRa+/-) or wildtype control mice bearing neither TGCre, nor PDGFRFa-Flox, following a previously reported method involving digestion with collagenase, and were used without sub-culturing (33). The dispersed cells were resuspended in Ham's F-12 medium containing 10% FBS and LFs were selected by their adherence to tissue culture dishes for 1h at 37^0C and approximately one-third of the adherent cells were PDGFRα-GFP+. The purity of the LF isolate was assessed by immunostaining for cellular markers specific for epithelial (anti-pan cytokeratin antibody), macrophage (CD 206) and endothelial (CD31) cells (36). Epithelial and endothelial cells comprised approximately 2.5 and 1.6 % respectively, whereas macrophages were only detected in the PDGFRα-GFP^{neg} population (36).

Primary fibroblast cell culture: The methods for culturing LF have been published (21) (33). Fibroblasts used for confocal microscopy were plated onto glass bottom dishes (MatTek, Ashland, MA), which had been coated with 10 μg/ml fibronectin peptide. For studies of cell migration fibroblasts were first cultured to near confluence on tissue culture plastic and then released using 0.25% Trypsin, 1 mM EDTA or TrypLE Express® and counted prior to re-plating in devices suitable for migration and imaging. Sixteen hours prior to adding the test reagents, the FBS concentration was reduced to 2% unless indicated otherwise.

Migration of confluent LF into an adjacent empty space. This assay used vitronectin-coated glass Stickyslides® (Ibidi,Verona, WI) fitted with silicone inserts that divide each well into two segments. Following removal of the insert a 500 μm gap remained and was unoccupied by cells at the beginning of time-lapse imaging. The details have been described (34). For the 16 hours prior to removing the insert,

157 the FBS concentration was reduced to 2%, which remained during imaging, when the HEPES
158 concentration was increased to 30 mM and some wells were supplemented with PDGF-A to 10 ng per ml.
159 The following inhibitors were dissolved in PBS added to the final concentrations: NSC23766 12.5 μM
160 (Rac1 GEF inhibitor), or Y27632 10 μM (Rho-activated kinase, ROCK inhibitor). The inhibitor
161 concentrations were chosen because preliminary experiments established that they were sufficient to yield
162 the expected effect, but did not weaken attachment of the cells to their substrate. Two additional
163 inhibitors were dissolved in DMSO which was diluted to 0.1% at the final inhibitor concentrations of 2
164 μM for U73122 (phospholipase Cγ inhibitor) or 25 μM LY29402, (phosphoinositide-3-kinase inhibitor).
165 The time lapse imaging commenced immediately after adding the inhibitors.

166 *Analysis of LF spreading on substrates of varying stiffness*. Easy coat Matrigen Softview™ gels were
167 incubated with 10 μg/ml fibronectin for 1 hour before adding fibroblasts. Fibroblasts isolated from
168 TGCre;PDGFRaF/F or littermate control mice were sub-cultured onto Softview™ hydrogels and
169 maintained for 16 h in Ham's F12 medium containing 10% FBS. The medium was changed so the
170 components were identical to those used for cell-migration imaging, and randomly selected fields were
171 imaged using DIC optics with an Olympus UPLFN20X:U PLAN objective and captured using an XM-10
172 monochrome CCD camera. Olympus CellSens™ software was used to trace the cellular perimeter s and
173 derive the areas. The cell shape factor, isoperimetric quotient: $4\pi A / P^2$ (P, perimeter, A area), was
174 calculated for each cell and expressed as a mean for each stiffness for control and PDGFRα-deleted cells
175 from three separate isolations for each genotype.

176 *Fabrication of soft-silicone substrates*. Thirty millimeter round coverglass was cleaned with detergent,
177 rinsed with deionized H2O , followed by acetone and ethanol, and then dried. Mixtures of Nusil 8100
178 silicone gel and Sylgard 184 (polydimethylsiloxane) were made with the following ratios: 18:1, 8 kPA;
179 12:1 10 kPA; and 5:1, 64 kPa). After degassing the mixtures were applied to the coverslides using a spin
180 coater turning at 800 rpm for the 5:1 and 600 rpm for the 12:1 and 18:1 mixtures, respectively. Sterile
181 MatTek dishes with a 20 mm diameter open bottom were placed on the silicone-coated coverslides and

adhered by baking at 70^{o} for 8 hours. The depth of the silicone layers was approximately 300 µm. Thicker gels with the same proportions of Nusil:PDMS were used to estimate the stiffness using either a Shore 00 or 000S durometer (Rex Gauge Co, Buffalo Grove, IL) (39). Prior to overlaying the collagen gel, the silicone gels were soaked in 100% ethanol overnight and two additional times for 1 h and then rendered hydrophilic by oxygen plasma treatment for 60 s in a PE-50 plasma cleaner, (PlasmaTech, Carson City, NV).

Fabrication of elastic fibers embedded in polyacrylamide gels. 100 x 25 mm #1.5 glass coverslides were cleaned using the procedure described for the 30 mm coverslides. After immersing in 5% NH4OH containing 3% H2O2, the coverslides were soaked overnight in 2% 3-aminopropyl triethoxysilane in 100% ethanol , followed by extensive rinsing in 100% ethanol followed by deionized H_2O. Prior to electrospinning the coverslides were immersed in 0.5% glutaraldehyde and air dried. Electrospinning was performed using a Gamma High Voltage power supply at 20kV attached to a metal needle, which was 20 cm from the cathode which housed the coverslide overlying a brass plate. A 10 mg/ml solution of alpha elastin, which had been prepared from bovine nuchal ligament was dissolved in 1,1,1,3,3,3-Hexafluoro-2-propanol and expelled the needle using a syringe pump with a flow rate of 50 µl per minute. The elastic fibers were maintained in the vapors of 25% glutaraldehyde overnight for cross-linking and then washed extensively with sterile H_2O prior to embedding in polyacrylamide. Polyacrylamide gels were prepared containing 10% acrylamide and 0.06% bis-acrylamide, and immediately after adding TEMED and ammonium persulfate, 90µl was applied to the coverslide which was partially occupied by the elastic fiber mat. A siliconized 24 X 75 mm, #2 coverslide was applied and after 30 minutes the siliconized coverslide was carefully removed. The gel was washed with 50 mM HEPES pH 8.5, and after carefully removing the excess buffer, 300 µl of a 1 mM solution of Sulfo-SANPAH (sulfosuccinimidyl 6-(4'-azido-2'-nitrophenylamino)hexanoate) in 50 mM HEPES pH 8.5 was applied. The polyacrylamide gel was irradiated twice for 3 minutes with 365 nM light with an intervening change of Sulfo-SANPAH. After removing the Sulfo-SANPAH, the gel was washed with 50 mM HEPES, followed by PBS and then

incubated overnight with a 200 mg/ml solution of bovine collagen (PureCol® InfaMed, Fremont CA) in PBS. The outer boundary of the coverslide was cleaned with sterile H2O, followed by isopropanol, and then Silane Glass Teatment AP115 3M Company, St. Paul, MN. A 6-well Ibidi sticky-Slide $^{0.4}$ (Ibidi Verona, WI) was applied and the edges were sealed with silicone sealant. The apparatus was irradiated for 30 min with UV light (280 nm), prior to rinsing the wells and adding fibroblasts.

Fibroblast durotaxis towards the elastic fiber mat. Lung fibroblasts were isolated from the lungs of mice bearing the PDGFRα-GFP gene insertion, and nuclear GFP was used to localize the cells during migration. At t he first sub-cultivation, 1.2 x 10^4 cells were added to each of the filling ports of the Ibidi sticky-Slide $^{0.4}$ which were distant from the region which contained the mat of elastic fibers. The cells were allowed to adhere and FBS concentration of the medium was reduced to 2%. Serial images were captured from four fields for each well at a consistent position that corresponded to between 1000 and 500 μm from the elastic fibers (34). The images were analyzed using Olympus CellSens® software to annotate the X and Y coordinates and distance traveled for every 30 minute interval and the speed and persistence were calculated (32).

Analysis of Rac1-activation using a Rac1-FRET biosensor. Lung fibroblasts were isolated from TGCre+/-;PDGFRαF/F or control mice and were used after the initial cultures reached 80% confluence. Culture dishes with a glass bottom (MatTek) were coated with 10 μg/ml fibronectin peptide or 200 μg/ml PureCol® collagen for two hours at room temperature or overnight at 4o. Lung fibroblasts were seeded at a density of 4.5 x 10^4 cells per cm^2 in Ham's F12 medium containing 10% FBS and cultured over night. The following day, the fibroblasts were transduced for 6h with the Rac1 biosensor in the Ad5CMV-adenoviral vector at a multiplicity of infection (MOI) of 3 in OptiMEM containing 3% FBS, and supplemented to 3 mM calcium, The pre-optimized multiplicity of infection (MOI) of 3. The low MOI was chosen because it transduced sufficient cells, but avoided overwhelming the endogenous Rac1 GEFs, GAPs, or GDIs. This ensured that the biosensor would accurately reflect the behavior of endogenous Rac1. Fibrillar collagen (Fibrocoll® 5133 Advanced Biomatrix, San Diego, CA) was added to the culture

medium 18 h prior to measuring Rac1-FRET, to fibroblasts which had been plated on collagen-coated glass.

To assess the effects of embedding in fibrillar collagen, fibroblasts were transduced at MOI =3 in the culture plates where they were placed after isolation. The virus was removed after 6 h and the cells were cultured overnight in OptiMEM containing 5% FBS, 3 mM Ca, 100U penicillin G, and 100 μg/ml streptomycin. The following day, the cells which were to be embedded in collagen gels were released for the culture plastic using TrypLE Express® (ThermoFisher, Waltham, MA). Fibrillar collagen was mixed with one-tenth volume of 10X PBS, Ham's F12 medium, and neutralized with 0.1 NaOH prior to adding 1 x 105 cells which were plated onto the 3.1 cm2 surface area of silicone substratum. Following incubation at 37^{o} for 45 minutes, OptiMEM medium containing 3% FBS was added and the gels were incubated for 18 h in at 37^{o} in 5% CO2. When assessing the effects of kinase inhibitors on Rac1-FRET the compounds were added 2 hours prior to measuring Rac1-FRET. Prior to imaging, the medium was changed to FluoBrite™ medium containing 2% FBS, 2 mg/ml BSA, 30 mM HEPES pH 7.3, 100U penicillin G, and 100 μg/ml streptomycin.

FRET imaging and data analysis. Imaging was conducted in an environmental chamber (37^{o} humidified 21% O_2, 7% CO_2, 71% N_2) using an Olympus IX81 inverted microscope, Excelitas X-Cite 120 LED light source, DIC optics, Hamamatsu OrcaR2 CCD camera, equipped with a Prior ProScan III controller used to change excitation (427/10-25, mCerulean and 504/12-25 mVenus) and emission (472/30-25 mCerulean and 542/27-25 mVenus) filters in Prior high speed filter wheels. Imaging conditions were optimized to limit excitation intensity and exposure time to reduce photobleaching. The LED light source provided very stable output so that the same exposure time could be used for all experiments. Cells with saturated pixels were avoided and cells were selected for imaging if their intensity was at the lower range of emission intensity that could be accurately analyzed. Images were captured using CellSens® software and then converted to TIFF format for analysis using pFRET Software and ImageJ plug-in available from University of Virginia (http://innovation.virginia.edu/). Regions of interest were only selected from the

cell periphery because the some cells exhibited nuclear fluorescence. At least 12 cells were imaged for each condition and were analyzed using both the pFRET (calculates FRET efficiency and Förster distance for each pixel) and rFRET (calculates pixel by pixel ratio of intensity in the FRET acceptor channel relative to the intensity in the donor emission channel after donor excitation). Data from all 12 cells for each condition were pooled and mean FRET intensities were calculated for each experiment. At least 4 experiments were conducted for each condition and N= the number of repetitions of each experiment. The Mlg2980 (ATCC CCL-206), neonatal mouse continuous cell line was transfected with plasmids containing either mCerulean or mVenus, images were captured using conditions identical to those for FRET analysis, and were used to calculate the spectral bleed through.

Co-localization of F-actin with talin and phospho-Paxillin in cultured LF. Fibroblasts obtained from the lungs of TGCre+/-;PDGFRαF/F or control mice were cultured on cleaned glass coverslips which had been coated with 10 μg/ml fibronectin to promote cell adhesion. The LF were allowed to adhere to the coverslips for 1 hour, non-adherent cells were removed by washing and the adherent LF were cultured overnight in Ham's F-12 medium containing 10% FBS. Sixteen hours prior to analysis the medium was changed to OptiMEM supplemented with 2.5% FBS, penicillin, streptomycin, containing OptiMEM-1 supplemented with 2.5 % FBS, with $CaCl_2$ to a final calcium concentration of 3 mM Ca^{+2}. Six hours prior to fixation with 2% paraformaldehyde at 4^{o}, the medium was changed and in some instances was supplemented with to 12.5 μM NSC23766, 10 μM Y27632, and/or 10 ng/ml PDGF-A. After permeabilization with 0.1% Triton X-100 and blocking with 5% normal donkey serum, the coverslips were incubated overnight with 1 μg/ml goat anti-talin and 0.24 μg/ml anti-phospho-paxillin and controls received goat or rabbit IgG, respectively at equivalent concentrations. Secondary antibodies were donkey anti-goat A647 or anti-rabbit IgG-A568 at 1:1000 or 1:2000dilutions respectively. Images were acquired at a 1024 x 1024 pixel density from randomly selected fields using Zeiss LSM710 confocal microscopes and a Zeiss Plan achromat 63x/1.40 Oil DIC M27 objective and averaged from three scans. The following excitation/emission filters were used: a 488/492-536 nm band pass filter to detect A488

phalloidin, a 547-590 nm band pass filter to detect Alexafluor 568-phospho-paxillin, and a 637-757 nm band pass filter for A647-talin. After washing, 100 nM A488 phalloidin was added for 30 minutes at room temperature. The uncompressed images were converted to TIF format and co-localization was analyzed using the JACoP plugin with Fiji (NIH Image2) software (37).

Proximity ligation assay (PLA) to assess Rac1-GEF interactions. To identify guanine nucleotide exchange factors (GFF)s which mediate signals from PDGF-A and collagen, we examined protein interactions between Dock180/ELMO and p130Cas, as well as interactions between β-PIX/GIT and paxillin using the proximity ligation assay (PLA), which identifies two proteins which both reside within a 40 nm radius. We used the DuoLink® (Olink Bioscience, Sigma Aldrich St. Louis, MO) kit following the manufacturer's instructions as previously detailed, with the following modifications (37). Some fibroblasts cultures were incubated for 2 h with inhibitors of PI3K (LY294002) or Src-kinase (PP2), and then stimulated for 10 minutes with medium containing 20 ng/ml PDGF-A with or without an inhibitor. After washing the cells were fixed for 15 minutes with 4% paraformaldehyde , 5 mM EGTA, 2 mM MgCl2, 80 mM PIPES pH 6.8, to preserve actin filaments (28). F-actin was stained with Acti-stain A488 phalloidin and nuclei with ToPro-3. We distinguished cytoplasmic granules which localized to the perinuclear region, which also contained ventral actin fibers from those within lamellipodia, which lack ventral actin fibers. We enumerated all cytoplasmic granules as well as those lying distal to the ends of ventral F-actin and within lamellipodia, which contained only subcortical and dorsal actin fibers.

Statistical methods: Box plots extend from the 25^{th} to the 75^{th} percentiles and whiskers were plotted based on the Tukey interquartile range using GraphPad Prism®. "N" is the number of different mice that were used or the number of different experiments that were performed using cell cultures (48). Analysis of variance (either 1 or 2-way as indicated in the figure legends) was performed using Systat (Chicago, IL) and Student's t-test using Microsoft Excel (either paired or unpaired as indicated in the figure legends). Additional details describing how the data from different images or image stacks were combined appears in the method for a particular stereological procedure. Values of $P < 0.05$ were considered significant.

Results

PDGFRα regulates fibroblast spreading on substrates of varied stiffness. Lung fibroblasts, which had been isolated from littermate control (without PDGFRα-deletion) mice demonstrated a stiffness-related increase in surface area and the shape factor was lower at 8 compared to 1 kPa, showing that control cells were more elongated and irregularly shaped on stiffer substrates. However the stiffness-related decrease in shape factor was not observed in LF from mice bearing a conditional deletion of PDGFRα (Fig. 1B). To determine whether mechanosensitive (stiffness-regulated) fibroblast spreading depends on Rho-kinase, fibroblasts from wildtype control mice were cultured in the presence and absence of Y27632, an inhibitor of Rho-activated kinase (ROCK). The inhibitor altered fibroblast-spreading, showing that PDGFRα interacts with Rho-GTPase to control cell shape (Fig. 1C).

PDGFRα confers responsiveness of LF migration to Rac1- and Rho-activated kinase inhibition. Time-lapse imaging was used to quantify the movement of fibroblasts from a confluent monolayer into an initially unoccupied space. The Rac1-GEF inhibitor, NSC23766, reduced the migration of littermate control, but did not alter the migration of PDGFRα-deficient fibroblasts (Fig. 2A). This demonstrates that PDGFRα is an important effector of Rac1-mediated signaling in murine LF. During cell migration, PDGFRα and Rac1 co-localize at the membrane of the leading edge (55). Two important membrane-associated -targets of PDGFRα-kinase are phosphinositide-3-kinase (PI3K) and phospholipase-Cγ (PlCγ), which both activate Rac1 (22). Either LY294002 (Figure 2B) or U73122 (Fig. 2C), selective inhibitors of PI3K and PLCγ, respectively, blocked the migration of control (without PDGFRα-deletion) fibroblasts after PDGF-A-stimulation. During migration, Rho-activated kinase stabilizes the ventral actin cytoskeleton, promotes adhesion, and transiently stabilizes the trailing edge (26). Although Y27632 did not affect control LF, it increased the migration of PDGFRα-deleted LF (Fig. 2D). Others have similarly observed that Y27632 increases the migration of Rac1-null mouse embryonic fibroblasts (50).

Focal adhesions are altered in LF from TGCre+/-;PDGFRaF/F mice. Migration on integrin-binding substrates such as fibronectin or collagen requires remodeling of focal adhesions, which transiently

anchor portions of the cell. When integrins engage extracellular ligands, talin and other intracellular actin-binding proteins, such as paxillin, are recruited to link cell-surface integrins to the sub-cortical cytoskeleton. By analyzing co-localized talin and actin, we examined how disruption of PDGFRα altered the abundance of focal adhesions and their destabilization by Y27632. In LF from TGCre+/-;PDGFRαF/F (PFlox) mice, the co-localization of talin with F-actin was significantly lower than in LF from littermates without deletion, both in the absence or presence of Y27632 (Fig. 3). Furthermore, Y27632 lowered co-localization of talin with F-actin in PDGFRα-deleted but not control LF, indicating that PDGFRα regulates focal adhesion-stability.

Because paxillin is phosphorylated during the remodeling of focal adhesions, we compared the co-localization of pY^{118}-paxillin and talin in control and TGCre+/-;PDGFRαF/F, both in the absence and presence of NSC23766. In both control and PDGFRα-deleted fibroblasts, inhibiting Rac1-activaton yielded more prominent talin-staining (Fig 4A). The Rac1-GEF inhibitor diminished co-localization of pY^{118}-paxillin with talin only in control fibroblasts (Fig. 4C), suggesting that Rac1 regulates focal adhesion turnover. This finding also argues that PDGFRα regulates focal adhesion turnover through Rac1. Likewise, others observed that Rac1-null mouse embryonic fibroblasts exhibit less abundant paxillin in focal contacts, which are more labile than those in Rac1-replete controls (50) (57).

Durotaxis of PDGFRα-expressing LF results from increased migrational persistence. Others have shown that durotaxis (migration towards a more rigid substrate) requires phasic remodeling of focal adhesions, where integrins, talin and vinculin interact to transiently strengthen the nexus between the extracellular matrix (ECM) and the cytoskeleton (10). To learn whether LF exhibited durotaxis, we devised soft polyacrylamide gels wherein a portion was stiffened by embedded elastic fibers (fig. 5A). In all wells, the cells were added to a softer (4 kPa) region of the gel. Some of the lanes ended where elastic fibers were embedded (32 kPa) whereas other lanes ended in regions devoid of elastic fibers (4 kPa). Using time-lapse imaging, we then compared the migration of PDGFRα-expressing fibroblasts (identified by nuclear GFP) in the two classes of lanes (4 kPa beginning and 4kPa end, versus 4 kPa beginning and 32 kPa end,

Fig. 5B). Following 24 h, more fibroblasts accumulated at the boundary proximate to elastic fibers (32 kPa) than in a 4 kPa region of the polyacrylamide gel located at the same distance from their entry well, but in a lane distant from the elastic fibers (Fig. 5C). After migrating towards the stiffer elastic fiber-laden sub-stratum, LF occupied a larger area with more protrusions (decreased shape factor, Fig. 5D), similar to the spreading of LF (Fig. 1). Time lapse imaging demonstrated that durotaxis of PDGFRα-expressing fibroblasts towards the 32kPa substratum resulted from greater directional persistence, rather than an increased speed of migration (Fig. 5E).

PDGFRα promotes Rac1-activation and attraction towards a stiffer substratum. Because PDGFRα regulates the turnover of focal adhesions, which is required for durotaxis, we studied how PDGF-A or mechanical stimuli alter Rac1-activation in LF. Others have shown that Rac1-mediates mechanosenstive responses (43). When GTP, rather than GDP is bound the Rac1-FRET biosensor, it undergoes a conformational change increasing the proximity between the mCerulean donor and mVenus acceptor, thereby enabling FRET (38).

As expected, PDGF-A increased Rac1-FRET in fibroblasts on fibronectin-coated glass (Fig. 6A). Because PDGFRα-regulated fibroblast spreading on collagen coated, soft polyacrylamide gels (Fig. 1), we studied whether fibrillar collagen-1 enhanced Rac1 FRET. Adding fibrillar collagen to the medium bathing fibroblasts on collagen-coated glass, increased Rac1-FRET (Fig. 6B), showing that collagen's effect is independent of substrate stiffness. The effect was concentration-dependent (Fig. 6B) and was greater when fibroblasts were embedded in a 2 mg/ml collagen gel (Fig. 6C). To further evaluate the interaction between collagen and sub-stratum-rigidity, we fabricated devices where fibroblasts could migrate from within a soft (approximately 0.2 kPa) collagen matrix towards a silicone substratum with varied stiffness (from 8 to 64 kPa). Rac1-FRET was analyzed in cells that accumulated near the interface between the collagen gel and the silicone sub-stratum. Rac1-FRET was higher in control fibroblasts adjacent to the 64kPa than either the 10 or 8 kPa sub-stratum, but this stiffness-related alteration of Rac1 activation was not observed in fibroblasts from TGCre+/-;PDGFRαF/F mice (Fig. 6D). The rFRET

intensity-map is shown in Fig. 6E for a collagen- embedded LF, which exhibited asymmetry of Rac1-GTP formation. To exclude a trivial explanation, we transfected MLg 2908 cells with a plasmid that expresses mCerulean, separated from mVenus by a 5 amino acid linker, yielding an ideal Förster radius for FRET. Embedding the MLg 2908 cells in a collagen gel did not alter the FRET/donor emission ratio indicating that collagen itself did not produce differential quenching at the donor wavelength (data not shown). These findings directly demonstrate that rigidity-responsive Rac1-activation requires PDGFRα-signaling, supporting the observations made using the Rac1-GEF inhibitor NSC23766 (Figs. 1 and 2). PDGF-A and collagen recruit Rac1-GEFs, including βPIX/GIT and Dock180/ELMO, to adapter molecules paxillin and p130Cas, respectively, located near the inner plasma membrane where Rac1 is also recruited (Fig. 6F).

Signaling pathways linking extracellular stimuli to intracellular Rac1. Next, we examined how PDGFRα- and integrin-linked kinases signal to the adapters and Rac1-GEFs shown in Fig. 6F. Knowing that PDGF-A increased migration via PI3K (Fig 2), and is a critical for PDGFRα-mediated Rac1 activation in other cells (16), we examined whether the PI3K-inibitor LY294002 decreases Rac1-FRET. Similarly, we used PP2, a specific inhibitor of Src-kinase (a known PDGFRα-target), to determine whether Src mediates Rac1-activation. Both LY294002 and PP2 prevented the augmentation of Rac1-FRET by PDGF-A when fibroblasts had adhered to fibronectin-coated glass (Fig. 7A). We then sought to identify Rac1-GEFs which are targeted by PI3K or Src, realizing that they may not be the exclusive mediators. We reasoned that after PDGF-A or collagen-treatment, the preferred signaling pathways could be identified by complex formation between Src or PI3K phosphorylation targets and their preferred Rac1-GEFs. Others used co- immunoprecipitation of transiently over-expressed recombinant Dock180, and Crk to evaluate Src-mediated Rac1-activation (12). However in our case, this approach was not feasible, because lipofection yields undesirable cytotoxicity and low-transfection efficiency in mouse primary LF. Therefore we used the proximity ligation assay (PLA) to probe interactions between adapters that are phosphorylated via PI3K or Src and stimulate Rac1-FRET by binding particular Rac1-

GEFs (Dock180 and βPIX). We reasoned that localization of granules (indicating association of a kinase-target adapter with a Rac1-GEF) to lamellipodia, would correlate with lamellipodial Rac1-activation, as exemplified in Fig. 7F. When LF were plated on fibronectin-coated glass, Src mediated the association of both Dock180/ELMO (Fig. 7B) or βPIX (Fig. 7C) with their respective signaling partners, p130Cas or paxillin (both associations were decreased by PP2). In contrast, PI3K (inhibited by LY294002) only mediated association between Dock180/ELMO and p130Cas (Fig. 7B). When LF were exposed to fibrillar collagen, as in Fig. 6B, only the Src-kinase inhibitor prevented the stimulation of Rac1-FRET by fibrillar collagen (Fig. 7D). Likewise, PP2 reduced associations between βPIX and paxillin suggesting that they are induced by Src-kinases (Fig 7E). Taken together, these findings indicate that Src-kinase activates Rac1through both Dock180/ELMO and βPIX/GIT, whereas PI3K primarily activates Rac1 through Dock180/ELMO.

Discussion

In 1996 Boström and associates proposed that PDGF-A signaling expanded the population of PDGFRα+ myofibroblast precursors, which then "spread" into the airspace and differentiated during secondary septation (5). Since this seminal finding, it has become clear that PDGF-A signaling also regulates the proliferation, survival, and migration of PDGFRα+ fibroblasts postnatally (33) (35). We have now shown that Rac1 mediates the responsiveness of PDGFRα-expressing LF to mechanical stimuli.

PDGFRα, integrins, talin, and mechanosensing. More rigid substrata promoted spreading (increased area) and lamellipodia formation (reduced shape factor, Fig. 1B), in PDGFRα-sufficient, but not PDGFRα-deficient fibroblasts, suggesting that PDGFRα is required for this mechanosensitive response. Rho-GTPase mediated this response, because ROCK-inhibition altered spreading in wildtype control LF (Fig. 1C). The link between PDGFRα and mechanosensation is likely multi-factorial. Integrins tether the ECM to cells, are the “first responders” to variation in substrate stiffness, and mechanical forces change their conformation. Matrix-engagement repositions β1-integrins so they contact talin, which changes configuration, enabling it to bind to vinculin and paxillin, which stabilize F-actin in the sub-cortical

cytoskeleton (59). Upon recruitment to talin, paxillin is tyrosine phosphorylated which exposes its SH2 domain to Crk, thereby recruiting p130Cas. The observation that PDGFRα regulates the effects of Rac1-GEF inhibition on paxillin-phosphorylation (Fig. 4) was substantiated by examination of tyrosine kinase-signaling pathways, which recruit Rac1-GEFs and regulate cell-migration (Fig. 7).

PDGFRα and the balance between Rho- and Rac-GTPases during LF migration. As expected, PDGF-A increased the outward migration of PDGFRα-sufficient, but not PDGFRα-deficient LF, from a confluent monolayer (Fig. 2A and D). Migration of PDGFRα-sufficient fibroblasts was suppressed by the Rac1-GEF inhibitor, NSC23766, which did not alter the migration of LF obtained from TGCre+/-;PDGFRαF/F mice, showing that PDGFRα signals through Rac1 (Fig 2A). The converse was observed when fibroblasts were exposed to the ROCK-inhibitor Y27632, which enhanced migration of PDGFRα-deficient fibroblasts (Fig. 2D). This is consistent with the paradigm that migration requires a balance between Rho-GTPase, which stabilizes focal adhesions at the trailing edge, and Rac1-GTPase which fosters remodelling of focal contacts at the leading edge (26). Although insufficient PDGFRα reduced remodeling at the leading edge, inhibition of Rho-signaling stimulated migration by weakening focal adhesions at the trailing edge. This notion is further supported by observing that co-localization of talin with actin (marker of focal adhesions) was significantly reduced by Y27632 in fibroblasts lacking but not in fibroblasts with sufficient PDGFRα (Fig. 3).

Lung fibroblast durotaxis on 2D-collagen substrates. We also observed that fibroblasts migrate 2-dimensionally towards the more rigid portion of a collagen-coated surface (Fig. 5). This migration (durotaxis) requires variable, reciprocating interactions between the plasma membrane and the extracellular matrix. β1-integrins probe their environment using low affinity interactions, and modify the conformation of their intracellular tails to engage talin (54). On less rigid substrates, this conformational change is transient and dissociation occurs quickly. The rate of dissociation is slowed when integrins contact more rigid substrates, sustaining the interaction between integrin and talin to enable reinforcement by adapter proteins such as vinculin and paxillin. This reinforcement increases the recruitment of α-

actinin or other bundling proteins (54). Durotaxis requires directional persistence, as well as sustained interactions between integrins and the ECM. On more rigid substrata, migrating PDGFRα-expressing fibroblasts showed greater directional persistence rather than increased speed (Fig. 5E). Rac1 is also required for lamellipodia formation, stabilization of focal contacts, and directionally persistent migration in a chemotactic gradient (50).

Tyrosine kinase signaling and Rac1-GEF recruitment. Rho-family GTPases influence and are affected by opposing processes, which control cell migration: tyrosine phosphorylation versus dephosphorylation, and by actin fiber remodeling (treadmilling and branch formation) versus stabilization (bundling and myosin-engagement). PDGFRα signals through PI3K or Src, to recruit Rac1-GEFs. Knowing that activated PDGFRα enhances Rac1 signaling (Fig. 6A), we examined Dock180 and βPIX, two Rac1-GEFs which have been linked to PDGFRα. Under the same experimental conditions, the Src-inhibitor PP2 incited a parallel reduction in both Rac1-GTP and apposition of Dock180/ELMO with p130Cas, or βPIX/GIT with paxillin. Likewise, PP2 suppressed augmentation of Rac1-GTP (FRET) by fibrillar collagen, and correspondingly reduced the apposition of βPIX/GIT with paxillin, upon stimulation by PDGF-A. Others have demonstrated that Src-kinases phosphorylate GIT, recruit βPIX/GIT to paxillin, activate lamellipodial Rac1, and promote branched actin remodeling (60) (64) (25). However, this is tempered by tyrosine phosphatases which dampen Src phosphorylation, in order to achieve both lamelipodial extension and directional persistence during migration (6) (61) (20).

Like Src, PI3K recruits Rac1-GEFs to the inner plasma membrane. The PI3K inhibitor LY294002 reduced both Rac1-GTP and apposition of Dock180/ELMO with p130Cas (Figs 7A and B). After binding PDGF-A, PDGFRα recruits class 1-PI3K with its p110α or p110β catalytic and p85 regulatory subunits (3). PI3K p110β then associates with prenylated Rac1 within lamellipodia and filopodia (8). Membrane-embedded PIP3,4,5 tethers Rac1-GEFs, including Dock180 to generate Rac1-GTP, which by binding PI3K, can in turn enhance PIP3K activity (30) (2) (29) (44). Using a human glioblastoma cell line with PDGFRα-gene amplifications, others showed that PDGF-A increased phosphorylation of Y^{1811}

in the Rac1-GEF, Dock180, and elevated Rac1-GTP through p130Cas (12).

Limitations of the proximity ligation assay (PLA) for the assessment of Rac1-GEF interactions. Using the PLA one can quantify protein-protein interactions, in individual cells, and compare regions within them. This allowed us to focus on interactions by Rac1-GEFs in lamellipodia, where Rac1 regulates cell migration. Compared to peripheral lamellipodia, granules were more abundant in the perinuclear and central cytoplasm, which we reasoned may be associated with the endoplasmic reticulum (ER). Using the PLA others have observed protein-proximity during vesicular transport from the ER (4). Therefore, we distinguished granules in lamellipodia, which contain dorsal actin fibers, from those located in the central region, which is demarcated by ventral actin fibers. The oligonucleotides used in the DuoLink® PLA link proteins which reside within a 40 nm radius, and unlike co-immunoprecipitation, the PLA does not require that the proteins directly contact. Another limitation is that by targeting known interactions of Rac1-GEFs in other mesenchymal cells, we excluded novel interactions, which could have been identified using an unbiased approach (31). Nevertheless, the PLA corroborated our findings using FRET microscopy, and showed that the PDGFRα-kinase targets, PI3K and Src both contribute to Rac1-activation.

How do collagen gels increase Rac1-GTP? Another novel finding was that collagen increases Rac1-GTP, identifying a mechanism through which the extracellular matrix may direct fibroblasts. Fibroblasts contact collagen through β1-integrins, which, along with Rac1GEFs, signal through talin/paxillin/p130Cas to increase Rac1-GTP (18). Exposing dermal fibroblasts to collagen gels increased focal adhesion kinase (FAK)-dependent p130Cas phosphorylation, which is required for gel contraction (56). Others have shown that engagement of collagen by β1-integrins stimulates FAK-mediated phosphorylation and increases Rac1-GTP (27). Rac1-FRET was also influenced by the stiffness of the substratum which interacted with the collagen gel (Fig. 6D). PDGFRα-signaling was important for the cellular responsiveness to stiffness, because greater stiffness did not increase Rac1-FRET using LF from TGCre+/-;PDGFRαF/F mice. Precisely how PDGFRα and collagen interact to regulate the

507 responsiveness of Rac1 to stiffness, remains unclear, but likely involves integrins and/or discoidin domain
508 receptor-2 (DDR2), which modifies Rac1 signaling in invadosomes (19).

509 *PDGFRα-expressing mesenchymal cells play unique roles in collagen homeostasis*. PDGFRα+ muscle
510 satellite cells can alter natively differentiate into adipocytic or myofibroblastic phenotypes. The fate is
511 determined by alternative PDGFRα exon-usage and the abundance of a resultant truncated receptor,
512 which promotes the adipocytic phenotype (40). When satellite cells abundantly express full-length
513 PDGFRα, they produce more collagen, replacing muscle with fibrotic tissue. Similarly PDGFRα-
514 signaling is required for neural crest cells to migrate into the anterior cranio-facial prominence and
515 generate a continuous collagen fiber network, which stabilizes the dermal-epidermal junction (11). In
516 adult mouse lung, fibroblasts with greater PDGFRα-gene expression also more abundantly expressed
517 fibrillar collagens (13).

518 *Collagen, rigidity, and the pathogenesis of pulmonary emphysema*. A growing literature suggests that
519 anisotropically distributed mechanical forces contribute to acinar distortion and the progression of
520 emphysema (53). Although the collagen-content is increased, its maldistribution raises lung compliance
521 in mice which received intratracheal pancreatic elastase and in humans with emphysema, (17) (14). After
522 instilling pancreatic elastase into murine lungs, Ito and co-workers observed that tissue damping (a
523 measure of force-dissipation, related to tissue viscosity) decreased proportionally less than elastance,
524 yielding increased hysteresivity at volumes exceeding functional residual capacity (17). They proposed
525 that although lung hydroxyproline increased, newly synthesized collagen was disordered and lacked
526 fibrillar interactions, which would normally reduce compliance at volumes approaching total lung
527 capacity (17). Disordered collagen fibers also may misdirect interstitial fibroblasts and prevent septal
528 repair. Ravikumar and associates observed that interstitial collagen increased in the remaining lung of
529 dogs following a 70% but not a 58% lung resection (45). Increased collagen was accompanied by failed
530 restoration of alveolar surface area following 70%, whereas 58% resection enabled greater restoration.
531 These findings support Ito and associates' hypothesis that an orderly collagen network is required for

alveolar restoration.

Because current treatments of emphysema and interstitial fibrosis fail to modify the distorted lung architecture, there is fervent interest in restoring gas-exchange function, by repopulating synthetic or reconditioned tissue scaffolds with multipotent cells. Although the extracellular architecture may guide cells, there is a parallel need to understand how mesenchymal progenitor cells perceive and respond to these guidance cues. Because PDGFRα-expressing alveolar fibroblasts can alternatively assume lipid-storage or myofibroblastic phenotypes, fine-tuning PDGFRα-signaling may help to both spatially and temporally guide fibroblasts to optimal locations for restoration of the air-blood interface.

Acknowledgement: We are grateful to Louis Hodgson, Albert Einstein University, New York, NY for kindly sharing the Rac1-biosensor. This study was funded by a Merit Review award from the Department of Veterans Affairs research service.

Figure Legends

Figure 1: *PDGFRα regulates mechano-responsive LF spreading*. (A) A schematized depiction of a migrating lung fibroblast (LF) showing the leading edge with a subcortical cytoskeleton, subtended by the Rac1-responsive Actin-related Protein 2 (Arp2) complex. Phospho-protein intermediates in the signaling pathway leading from PDGFRα to Rac1-GTP are shown. GIT, G-protein coupled receptor kinase interacting protein; βPIX, p21-activated-kinase interacting exchange factor-β, also named Rho Guanine nucleotide exchange factor 7; p130Cas (BCAR1), breast cancer anti-estrogen resistance protein-1 (Cas family adapter protein); Dock180 (Dock1), Dedicator of cytokinesis; ELMO Engulfment and Cell Motility protein-1. (B) LF were isolated from TGCre+/-;PDGFRαF/F or littermate TGCre+/-;PDGFRα F/- control mice and adhered to fibronectin-coated polyacrylamide gels of varying stiffness (kPa, kiloPascal) for 16 hours. Cellular outlines captured using DIC were traced to ascertain the area, perimeter, and shape factor (isoperimetric quotient) $4\pi A / P^2$ (P, perimeter, A area), which is smaller in more elongated and irregularly shaped cells. Boxes extend from the 25^{th} to the 75^{th} percentile and whiskers are based on the Tukey interquartile range, showing 20 cells from a representative isolation, dots are outliers. N=3 cell isolations. (*) $P<0.05$ comparing PDGFRα- deleted to TGCre+/-;PDGFRα F/- control LF at the same substrate stiffness. (†) $p<0.05$ comparing 1 to 8 or 25 kPa within TGCre+/-;PDGFRα F/- control group. (**) $p<0.05$ comparing 8 to 25 kPa within TGCre+/-;PDGFRα F/- control group. (†) $p<0.05$ comparing 1 to 8 or 25 kPa within the TGCre+/-;PDGFRα F/- control group. One-way ANOVA on ranks. (C) Primary LF from 3 wildtype control mice were cultured as in A, except during the last 6 hours the medium in some wells also contained 10 μM Y27632, a Rho-associated protein kinase inhibitor. (*) $P<0.05$, comparing Y27632-treated to control LF at the same substrate stiffness, dots are outliers. One-way ANOVA on ranks. (†) $p<0.05$ comparing 1 to 8 kPa within control group.

Figure 2: *PDGFRα-signaling promotes lung fibroblast (LF) migration*. (A) LF were isolated from the lungs of TGCre+/-;PDGFRαF/F or littermate TGCre+/-;PDGFRα F/- control mice and adhered to vitronectin-coated glass within 8-well StickySlide® chambers. Removing the sub-well insert left an

intervening empty space into which the LF migrated in the presence or absence of PDGF-A or NSC23766, a selective Rac1-GEF-inhibitor. The cumulative number of cells which had entered the previously empty space is plotted at one hour intervals. Mean ± SEM, n=3 separate cell isolations for each genotype, (*) $P<0.05$, repeated measures ANOVA, compared to control (medium containing 2% FBS). (B) Primary LF from 3 wildtype control mice were cultured as in A, except during migration, some wells contained either the phosphoinositide 3-kinase inhibitor LY294002, or (C) the phospholipase-Cγ inhibitor U73211. (D) TGCre+/-;PDGFRα F/- control or PDGFRα-deleted LF were cultured under similar conditions except that Y27632 was used as an inhibitor of Rho-activated kinase. (*) $P<0.05$, repeated measures ANOVA, compared to control (medium containing 2% FBS).

Figure 3: *PDGFRα signaling regulates focal adhesion formation in LF*. (A) LF from TGCre+/-; PDGFRαF/F or TGCre+/-;PDGFRα F/- control mice were adhered to fibronectin-coated glass, and after reducing the concentration of FBS to 2%, the cells were incubated for 6 h in the presence or absence of 10 μM Y27632 (Rho-kinase inhibitor). After fixation, the sub-confluent cell layers were stained for F-actin (green) or talin (blue) and imaged using the LSM 710. Inset is a line scan over a representative region to show co-localization of talin and F-actin in pixels intersected by the line. (B) Using data from three separate experiments the Manders' coefficient-2 (M2) for co-localization of talin in pixels containing actin was determined using the JACoP plug-in (Fuji, Image J2). Box and whisker (Tukey) plots combining 4 separate cell isolations. $P<0.05$, comparing TGCre+/-; PDGFRαF/F to TGCre+/-;PDGFRα F/- control LF, or effect of Y27632 on TGCre+/-; PDGFRαF/F LF; 2-way ANOVA.

Figure 4: *PDGFRα and Rac1 regulate .localization of phospho-paxillin to focal adhesions*. (A) LF were isolated and cultured as in Figure 3 except that the Rac1-GEF inhibitor NSC23766 was added for 6 h prior to fixation. In addition to actin and talin, phosphoY^{118}-paxillin (pPax) was immunostained (red). Representative fields are shown from one experiment which yielded results similar to 3 additional experiments. Inset is a line scan over a representative region to show co-localization of pPax, talin and F-actin in pixels intersected by the line. (B) The Manders' coefficients M1, talin co-localized in pixels

containing pPax ,and M2, pPax co-localized in pixels containing talin were calculated . TGCre+/-;PDGFRαF/F LF were compared to those from littermate TGCre+/-;PDGFRα F/- controls, both in the presence and absence of NSC23766. Box and whisker (Tukey) plots including 4 separate cell isolations for each genotype. $p<0.05$ comparing NSC23766-treated to untreated LF from TGCre+/-;PDGFRα F/- control or TGCre+/-;PDGFRαF/F mice, two-way ANOVA.

Figure 5: *LF exhibit durotaxis on soft polyacrylamide substrates*. (A) Bovine α-elastin was electrospun into a randomly oriented, rectangular mat (phase-contrast image in A) on a glass coverslide, which was covered with a polyacrylamide gel, so that the central portion assimilated with the elastic fibers (stippled gray rectangle in lanes 3 through 5 in A). The gel-stiffness was dependent on the proximity to the elastic fibers which were present at the end of wells 3 through 5 (32 kPa) , but not wells 1, 2 and 6 (3 kPa). After adding LF from PDGFRα-GFP mice to the wells (shown at bottom in A), time-lapse images were captured to enumerate the cells which accumulated in a zone near the boundary with the elastic fiber mat (shown as a rectangle in upper portion of A). (B) Representative fields within this zone are shown, which were distant from (control) or proximate to (elastic fibers), with the perimeter of some cells outlined in white. (C) When the migration period ended, the LF in an equal area within the stippled rectangle (A) were enumerated in lanes which were distant from (1, 2 and 6), or proximate to (3, 4, and 5) elastic fibers. Box and whisker (Tukey) plot combining 7 separate cell isolations. (*) $P<0.01$ Student's t-test paired variables, comparing lanes with and without elastin. (D) Using the perimeters as illustrated in B, the areas and shape factors for LF within the zone were compared for control and elastic fiber containing lanes. Box and whisker (Tukey) plots combining 3 separate migration experiments (*) $p<0.05$ comparing wells with elastic fibers to control wells (Student's t-test for paired variables). (E) Thirty cells were analyzed within the regions distant from (control) or proximate to elastic fibers (elastin). Speed (S) and persistence (P) were calculated for each cell using the equation $D^2= S^2P^2(T/P-1 +e^{-T/P})$. D^2 is the square of the distance moved in the preceding 1 h (squared displacement in μm^2); P is the persistence time in hours, T is time in hours, and S is speed or velocity in μm per hour. Student's t-test, unpaired variables. Box

620 and whisker (Tukey) plots, dots are outliers. P<0.01 comparing elastin to control.

621 **Figure 6:** *PDGFRα promotes mechanosensitive Rac1-activation*. (A) Primary LF from control mice
622 were plated on fibronectin-coated glass and 16 h prior to imaging, the FBS concentration was reduced to
623 3%. After a 5 minute delay, images were acquired for 15 minutes in the absence (control) or presence of
624 50 ng/ml PDGF-A (PDGF-A). Y-axis is the mean pixel by pixel ratio for the intensity of the FRET
625 versus the donor channel within all regions of interest (ROI) at the periphery, for a particular cell. Box
626 and whisker (Tukey) plots combining 6 separate cell isolations, with pooled data from 12 cells per
627 condition, for each isolation. (*) P<0.01, Student's t-test, paired variables. (B) Primary LF from
628 wildtype control mice were plated on type 1collagen-coated glass and fibrillar collagen (at the
629 concentrations shown) was added to the medium when the serum concentration was reduced. Twelve
630 images were acquired for each collagen concentration, using 5 separate LF isolations and the data were
631 analyzed as in A. Box and whisker (Tukey) plots, (*) P<0.05, 1-way ANOVA. (C) Primary LF from
632 wildtype control mice were plated on collagen coated glass as in B, or embedded in a 2 mg/ml collagen
633 gel. After 16 h in medium containing 3% FBS, LF near the interface between collagen and glass were
634 imaged. LF plated on collagen-coated glass with 0.1 mg/ml collagen in the medium (as in B) were
635 compared to LF embedded within the collagen gel. Box and whisker (Tukey) plots combining 5 separate
636 cell isolations, (*) P<0.05, Student's t-test paired variables. (D) LF from TGCre+/-;PDGFRαF/F or
637 littermate control mice were embedded in 2 mg/ml collagen overlying a coverglass coated with an
638 approximately 300 μm layer of silicone gel with varying stiffness shown in kPa. After allowing 16 h for
639 the LF to migrate towards the silicone layer, 12 cells from each source were imaged and data were pooled
640 for 5separate cell isolations from mice of each genotype. Box and whisker (Tukey) plots, (*) P < 0.05, 2-
641 way ANOVA comparing varying stiffness within controls. (†) P<0.05, 2-way ANOVA comparing LF
642 from TGCre+/-;PDGFRαF/F (left panel) to those from littermate TGCre+/-;PDGFRαF/- control (right
643 panel) mice plated on 64 kPa silicone gels. (E) Map of regional Rac1-biosensor activity in a LF
644 embedded in a 2 mg/ml collagen, shows greater generation of Rac1-GTP in lamellipodia at the right side

of the image. (F) Diagram depicting the topography of PDGFRα or integrin initiated phosphorylation (through Src of PI3K) recruitment of the adapters paxillin or p130Cas, which then associate with the Rac1-GEFs βPIX or p130Cas and their respective binding partners, GIT or ELMO, to elevate Rac1-GTP .

Figure 7: *Downstream signaling pathways contributing to Rac1-activation*. (A) Eighteen hours following viral transduction of wildtype control LF adherent to fibronectin-coated glass, the FBS concentration was reduced to 3%, and after an additional 24 h the medium in some wells was supplemented with 4 μM PP2 or 25 μM LY294002 (LY294). After an additional 2 h, the medium remained usupplemented (control) or was supplemented with 50 ng/ml PDGF-A in the presence of absence of inhibitors. Rac-1-FRET was analyzed in at least 10 cells from 5 to 20 minutes after adding PDGF-A. N=4 separate cell isolations for each condition, (*) $P<0.05$ compared to untreated control; (†) $P<0.05$ compared to PDGF without inhibitor, 2-way ANOVA. Panels A, C and E show box and whisker (Tukey) plots, whereas Panels B and D show scatter plots for data, which were too concordant to be represented by boxes. (B, C and E) Proximity ligation assays (PLA) were performed to assess how inhibition of PI3K or Src-kinase altered the association of Rac1-GEFs and their binding partners (Dock180/ELMO or βPIX/GIT) with downstream targets, which mediate the effects of Rac1 on the cytoskeleton or integrins. (B) Association between Dock180/ELMO and p130Cas, n=3 cell isolations, total numbers of cells analyzed were 29, 31, 33, 29 for control, PDGF, PP2, and LY294, respectively. (C) Association between βPIX/GIT and paxillin, n=4 cell isolations, total numbers of cells analyzed were 44, 51, 40, and 46 for control, PDGF, PP2, and LY294, respectively using LF plated on fibronectin, as in A. The percentages of granules in lamellipodia relative to the total numbers of granules in that cell were plotted. For B and C, (*) $P<0.05$ comparing control in absence of PDGF-A or inhibitor to PDGF-A. (†) $p<0.05$ comparing PDGF-A and PP2 or LY294002 (LY294) treated LF to treatment with only PDGF-A, two-way ANOVA. (D) LF were added to collagen coated-glass and 18 h prior to analyzing Rac1-FRET, the FBS concentration was reduced to 3% and during the subsequent 24 h, the medium was supplemented with 100 μg of fibrillar collagen per ml; and some wells contained kinase-inhibitors during the last 2 h,

as in B. Some cultures received neither collagen nor inhibitors. Rac1-FRET was assessed as in Fig. 7A. (E) PLA analyzing association between βPIX/GIT and paxillin using LF cultured with the same substratum described in panel D. n=4 cell isolations, 44, 56, 49 cells analyzed for control, PDGF, and PP2, respectively. $P<0.05$ comparing control in absence of PDGF-A or inhibitor to PDGF-A. (†) $p<0.05$ comparing PDGF-A and PP2 treated LF to only PDGF-A treatment, two-way ANOVA. However, unlike Rac1-FRET shown in D, PDGF-A was required to detect differences in the association of Rac1-GEFs and downstream effectors using the PLA. (*) $P<0.05$ comparing control in absence of PDGF-A or inhibitor to PDGF-A. (F) Representative images of LF on fibronectin, which had been exposed to PDGF-A, or remained unexposed (control). F-actin was stained with A488-phalloidin (green), nuclei with ToPro-3 (blue) and PLA granules showing proximity between βPIX and paxillin are red.

References

1. **Abraham T and Hogg J**. Extracellular matrix remodeling of lung alveolar walls in three dimensional space identified using harmonic generation and multiphoton excitation fluorescence. *J Structural Biol* 171: 189-196, 2010.
2. **Barrows D, He JZ and Parsons R**. PREX1 Protein Function Is Negatively Regulated Downstream of Receptor Tyrosine Kinase Activation by p21-activated Kinases (PAKs). *J Biol Chem* 291: 20042-20054, 2016.
3. **Baumer AT, Ten FH, Sauer H, Wartenberg M, Kappert K, Schnabel P, Konkol C, Hescheler J, Vantler M and Rosenkranz S**. Phosphatidylinositol 3-kinase-dependent membrane recruitment of Rac-1 and p47phox is critical for alpha-platelet-derived growth factor receptor-induced production of reactive oxygen species. *J Biol Chem* 283: 7864-7876, 2008.
4. **Blanco-Sanchez B, Clement A, Fierro J, Jr., Washbourne P and Westerfield M**. Complexes of Usher proteins preassemble at the endoplasmic reticulum and are required for trafficking and ER homeostasis. *Dis Model Mech* 547-559, 2014.
5. **Boström H, Willetts K, Pekny M, Leveen P, Lindahl P, Hedstrand H, Pekna M, Hellstrom M, Gebre-Medin S, Schalling M, Nilsson M, Kurland S, Tornell J, Heath JK and Betsholtz C**. PGDF-A signaling is a critical event in lung alveolar myofibroblast development and alveogenesis. *Cell* 85: 863-873, 1996.
6. **Burdisso JE, Gonzalez A and Arregui CO**. PTP1B promotes focal complex maturation, lamellar persistence and directional migration. *J Cell Sci* 126: 1820-1831, 2013.
7. **Burri PH**. Structural aspects of postnatal lung development-alveolar formation and growth. *Biol Neonate* 89: 313-322, 2006.
8. **Das S, Yin T, Yang Q, Zhang J, Wu YI and Yu J**. Single-molecule tracking of small GTPase Rac1 uncovers spatial regulation of membrane translocation and mechanism for polarized signaling. *Proc Natl Acad Sci U S A* 112: E267-E276, 2015.

9. **Davila RM, deMello D and Crouch EC**. Ontogeny of type I procollagen expression during human fetal lung development. *Am J Physiol* 268: L309-L320, 1995.
10. **Elosegui-Artola A, Oria R, Chen Y, Kosmalska A, Perez-Gonzalez C, Castro N, Zhu C, Trepat X and Roca-Cusachs P**. Mechanical regulation of a molecular clutch defines force transmission and transduction in response to matrix rigidity. *Nat Cell Biol* 18: 540-548, 2016.
11. **Fantauzzo KA and Soriano P**. PDGFRbeta regulates craniofacial development through homodimers and functional heterodimers with PDGFRalpha. *Genes & Dev* 30: 2443-2458, 2016.
12. **Feng H, Hu B, Liu KW, Li Y, Lu X, Cheng T, Yiin JJ, Lu S, Keezer S, Fenton T, Furnari FB, Hamilton RL, Vuori K, Sarkaria JN, Nagane M, Nishikawa R, Cavenee WK and Cheng SY**. Activation of Rac1 by Src-dependent phosphorylation of Dock180(Y1811) mediates PDGFRalpha-stimulated glioma tumorigenesis in mice and humans. *J Clin Invest* 121: 4670-4684, 2011.
13. **Green J, Endale M, Auer H and Perl AK**. Diversity of Interstitial Lung Fibroblasts Is Regulated by Platelet-Derived Growth Factor Receptor alpha Kinase Activity. *Am J Respir Cell Mol Biol* 54: 532-545, 2016.
14. **Hamakawa H, Bartolak-Suki E, Parameswaran H, Majumdar A, Lutchen KR and Suki B**. Structure-function relations in an elastase-induced mouse model of emphysema. *Am J Respir Cell Mol Biol* 45: 517-524, 2011.
15. **Hamilton TG, Klinghoffer RA, Corrin PD and Soriano P**. Evolutionary divergence of platelet derived growth factor alpha receptor signaling mechanisms. *Mol Cell Biol* 23: 4013-4025, 2003.
16. **He F and Soriano P**. A critical role for PDGFRalpha signaling in medial nasal process development. *PLoS Genet* 9: e1003851, 2013.
17. **Ito S, Ingenito EP, Brewer KK, Black LD, Parameswaran H, Lutchen KR and Suki B**. Mechanics, nonlinearity, and failure strength of lung tissue in a mouse model of emphysema: possible role of collagen remodeling. *J Appl Physiol* 98: 503-511, 2005.
18. **Janostiak R, Pataki AC, Brabek J and Rosel D**. Mechanosensors in integrin signaling: the emerging role of p130Cas. *Eur J Cell Biol* 93: 445-454, 2014.

19. **Juin A, Di MJ, Leitinger B, Henriet E, Gary AS, Paysan L, Bomo J, Baffet G, Gauthier-Rouviere C, Rosenbaum J, Moreau V and Saltel F**. Discoidin domain receptor 1 controls linear invadosome formation via a Cdc42-Tuba pathway. *J Cell Biol* 207: 517-533, 2014.
20. **Karginov AV, Tsygankov D, Berginski M, Chu PH, Trudeau ED, Yi JJ, Gomez S, Elston TC and Hahn KM**. Dissecting motility signaling through activation of specific Src-effector complexes. *Nat Chem Biol* 10: 286-290, 2014.
21. **Kimani PW, Holmes AJ, Grossmann RE and McGowan SE**. PDGF-Rα gene expression predicts proliferation, but PDGF-A suppresses transdifferentiation of neonatal mouse lung myofibroblasts. *Respir Res* 10: 19, 2009.
22. **Klinghoffer RA, Hamilton TG, Hoch R and Soriano P**. An allelic series at the PDGFalphaR locus indicates unequal contributions of distinct signaling pathways during development. *Dev Cell* 2: 103-113, 2002.
23. **Koh DW, Roby JD, Starcher B, Senior RM and Pierce RA**. Postpneumonectomy lung growth: a model of reinitiation of tropoelastin and type I collagen production in a normal pattern in adult rat lung. *Am J Respir Cell Mol Biol* 15: 611-623, 1996.
24. **Kulkarni T, O'Reilly P, Antony VB, Gaggar A and Thannickal vJ**. Matrix Remodeling in Pulmonary Fibrosis and Emphysema. *Am J Respir Cell Mol Biol* 54: 751-760, 2016.
25. **Kuo JC, Han X, Hsiao CT, Yates JR, III and Waterman CM**. Analysis of the myosin-II-responsive focal adhesion proteome reveals a role for beta-Pix in negative regulation of focal adhesion maturation. *Nat Cell Biol* 13: 383-393, 2011.
26. **Lawson CD and Burridge K**. The on-off relationship of Rho and Rac during integrin-mediated adhesion and cell migration. *Small GTPases* 5: e27958, 2014.
27. **Leask A**. Integrin beta1: A Mechanosignaling Sensor Essential for Connective Tissue Deposition by Fibroblasts. *Adv Wound Care (New Rochelle)* 2: 160-166, 2013.

28. **Leyton-Puig D, Kedziora KM, Isogai T, van den Broek B, Jalink K and Innocenti M**. PFA fixation enables artifact-free super-resolution imaging of the actin cytoskeleton and associated proteins. *Biol Open* 5: 1001-1009, 2016.

29. **Lu HL, Chen SS, Hsu WT, Lu YC, Lee CC, Wu TS and Lin ML**. Suppression of phospho-p85alpha-GTP-Rac1 lipid raft interaction by bichalcone analog attenuates cancer cell invasion. *Mol Carcinog* 55: 2106-2120, 2016.

30. **Lucato CM, Halls ML, Ooms LM, Liu HJ, Mitchell CA, Whisstock JC and Ellisdon AM**. The Phosphatidylinositol (3,4,5)-Trisphosphate-dependent Rac Exchanger 1.Ras-related C3 Botulinum Toxin Substrate 1 (P-Rex1.Rac1) Complex Reveals the Basis of Rac1 Activation in Breast Cancer Cells. *J Biol Chem* 290: 20827-20840, 2015.

31. **Marei H, Carpy A, Woroniuk A, Vennin C, White G, Timpson P, Macek B and Malliri A**. Differential Rac1 signalling by guanine nucleotide exchange factors implicates FLII in regulating Rac1-driven cell migration. *Nat Commun* 7: 10664, 2016.

32. **McGowan SE, Holmes AJ, Mecham RP and Ritty TM**. Arg-Gly-Asp-containing domains of fibrillins-1 and -2 distinctly regulate lung fibroblast migration. *Am J Respir Cell Mol Biol* 38: 435-445, 2008.

33. **McGowan SE and McCoy DM**. Fibroblasts expressing PDGF-receptor-alpha diminish during alveolar septal thinning in mice. *Pediatr Res* 70: 44-49, 2011.

34. **McGowan SE and McCoy DM**. Platelet-derived growth factor-A and sonic hedgehog signaling direct lung fibroblast precursors during alveolar septal formation. *Am J Physiol Lung Cell Mol Physiol* 305: L229-L239, 2013.

35. **McGowan SE and McCoy DM**. Platelet-derived growth factor-A regulates lung fibroblast S-phase entry through p27(kip1) and FoxO3a. *Respir Res* 14: 68, 2013.

36. **McGowan SE and McCoy DM**. Regulation of fibroblast lipid storage and myofibroblast phenotypes during alveolar septation in mice. *Am J Physiol Lung Cell Mol Physiol* 307: L618-L631, 2014.

37. **McGowan SE and McCoy DM**. Fibroblast growth factor signaling in myofibroblasts differs from lipofibroblasts during alveolar septation in mice. *Am J Physiol Lung Cell Mol Physiol* 309: L463-L474, 2015.

38. **Miskolci V, Wu B, Moshfegh Y, Cox D and Hodgson L**. Optical Tools To Study the Isoform-Specific Roles of Small GTPases in Immune Cells. *J Immunol* 196: 3479-3493, 2016.

39. **Mix AJ and Giacomin AJ**. Standardized polymer durometry. *J Testing Evaluation* 39: 696-705, 2011.

40. **Mueller AA, van Velthoven CT, Fukumoto KD, Cheung TH and Rando TA**. Intronic polyadenylation of PDGFRalpha in resident stem cells attenuates muscle fibrosis. *Nature* 540: 276-279, 2016.

41. **Oldmixon EH, Carlsson K, Kuhn C, III, Butler JP and Hoppin FG, Jr.** alpha-Actin: disposition, quantities, and estimated effects on lung recoil and compliance. *J Appl Physiol* 91: 459-473, 2001.

42. **Oliveira MV, Abreu SC, Padilha GA, Rocha NN, Maia LA, Takiya CM, Xisto DG, Suki B, Silva PL and Rocco PR**. Characterization of a Mouse Model of Emphysema Induced by Multiple Instillations of Low-Dose Elastase. *Front Physiol* 7: 457, 2016.

43. **Pasapera AM, Plotnikov SV, Fischer RS, Case LB, Egelhoff TT and Waterman CM**. Rac1-dependent phosphorylation and focal adhesion recruitment of myosin IIA regulates migration and mechanosensing. *Curr Biol* 25: 175-186, 2015.

44. **Premkumar L, Bobkov AA, Patel M, Jaroszewski L, Bankston LA, Stec B, Vuori K, Cote JF and Liddington RC**. Structural basis of membrane targeting by the Dock180 family of Rho family guanine exchange factors (Rho-GEFs). *J Biol Chem* 285: 13211-13222, 2010.

45. **Ravikumar P, Yilmaz C, Dane DM, Bellotto DJ, Estrera AS and Hsia CC**. Defining a stimuli-response relationship in compensatory lung growth following major resection. *J Appl Physiol (1985)* 116: 816-824, 2014.

46. **Rishikof DC, Lucey EC, Kuang PP, Snider GL and Goldstein RH**. Induction of the myofibroblast phenotype following elastolytic injury to mouse lung. *Histochem Cell Biol* 125: 527-534, 2006.

47. **Roan E and Waters CM**. What do we know about mechanical strain in lung alveoli? *Am J Physiol Lung Cell Mol Physiol* 301: L625-L635, 2011.
48. **Rosner B**. *Fundamentals of Biostatistics*. Boston: PWS-Kent Publishing Co., 1990,
49. **Sirianni FE, Milaninezhad A, Chu FS and Walker DC**. Alteration of fibroblast architecture and loss of basal lamina apertures in human emphysematous lung. *Am J Respir Crit Care Med* 173: 632-638, 2006.
50. **Steffen A, Ladwein M, Dimchev GA, Hein A, Schwenkmezger L, Arens S, Ladwein KI, Margit HJ, Schur F, Victor SJ, Schwarz J, Gerhard R, Faix J, Stradal TE, Brakebusch C and Rottner K**. Rac function is crucial for cell migration but is not required for spreading and focal adhesion formation. *J Cell Sci* 126: 4572-4588, 2013.
51. **Stolz D, Leeming DJ, Kristensen JH, Karsdal MA, Boersma W, Louis R, Milenkovic B, Kostikas K, Blasi F, Aerts J, Sand JM, Wouters EF, Rohde G, Prat C, Torres A, Welte T, Roth M, Papakonstantinou E and Tamm M**. Systemic Biomarkers of Collagen and Elastin Turnover Are Associated With Clinically Relevant Outcomes in COPD. *Chest* 151: 47-59, 2017.
52. **Stone PJ, Gottlieb DJ, O'Connor GT, Ciccolella DE, Breuer R, Bryan-Rhadfi J, Shaw HA, Franzblau C and Snider GL**. Elastin and collagen degradation products in urine of smokers with and without chronic obstructive pulmonary disease. *Am J Respir Crit Care Med* 151: 952-959, 1995.
53. **Suki B, Sato S, Parameswaran H, Szabari MV, Takahashi A and Bartolak-Suki E**. Emphysema and mechanical stress-induced lung remodeling. *Physiology (Bethesda)* 28: 404-413, 2013.
54. **Swaminathan V and Waterman CM**. The molecular clutch model for mechanotransduction evolves. *Nat Cell Biol* 18: 459-461, 2016.
55. **Takahashi M, Rikitake Y, Nagamatsu Y, Hara T, Ikeda W, Hirata K and Takai Y**. Sequential activation of Rap1 and Rac1 small G proteins by PDGF locally at leading edges of NIH3T3 cells. *Genes Cells* 13: 549-569, 2008.
56. **Takeya M, Okumura Y and Nikawa T**. Modulation of cutaneous extracellular collagen contraction by phosphorylation status of p130Cas. *J Physiol Sci* 2016.

57. **Thievessen I, Fakhri N, Steinwachs J, Kraus V, McIsaac RS, Gao L, Chen BC, Baird MA, Davidson MW, Betzig E, Oldenbourg R, Waterman CM and Fabry B**. Vinculin is required for cell polarization, migration, and extracellular matrix remodeling in 3D collagen. *FASEB J* 29: 4555-4567, 2015.

58. **Wasowicz M, Yokoyama S, Kashima K and Nakayama I**. The connective tissue compartment in the terminal region of the developing rat lung. An ultrastructural study. *Acta Anat (Basel)* 156: 268-282, 1996.

59. **Wehrle-Haller B**. Assembly and disassembly of cell matrix adhesions. *Curr Opin Cell Biol* 24: 569-581, 2012.

60. **Yu JA, Deakin NO and Turner CE**. Paxillin-kinase-linker tyrosine phosphorylation regulates directional cell migration. *Mol Biol Cell* 20: 4706-4719, 2009.

61. **Yu JA, Deakin NO and Turner CE**. Emerging role of paxillin-PKL in regulation of cell adhesion, polarity and migration. *Cell Adh Migr* 4: 342-347, 2010.

62. **Zhang J, Zhong W, Cui T, Yang M, Hu X, Xu K, Xie C, Xue C, Gibbons GH, Liu C, Li L and Chen YE**. Generation of an adult smooth muscle cell-targeted Cre recombinase mouse model. *Arterioscler Thromb Vasc Biol* 26: e23-e24, 2009.

63. **Zhang K, Rekhter MD, Gordon D and Phan SH**. Myofibroblasts and their role in lung collagen gene expression during pulmonary fibrosis. *Am J Pathol* 145: 114-125, 1994.

64. **Zhang X, Moore SW, Iskratsch T and Sheetz MP**. N-WASP-directed actin polymerization activates Cas phosphorylation and lamellipodium spreading. *J Cell Sci* 127: 1394-1405, 2014.

65. **Zhou Y, Huang X, Hecker L, Kurundkar D, Kurundkar A, Liu H, Jin TH, Desai L, Bernard K and Thannickal vJ**. Inhibition of mechanosensitive signaling in myofibroblasts ameliorates experimental pulmonary fibrosis. *J Clin Invest* 123: 1096-1108, 2013.

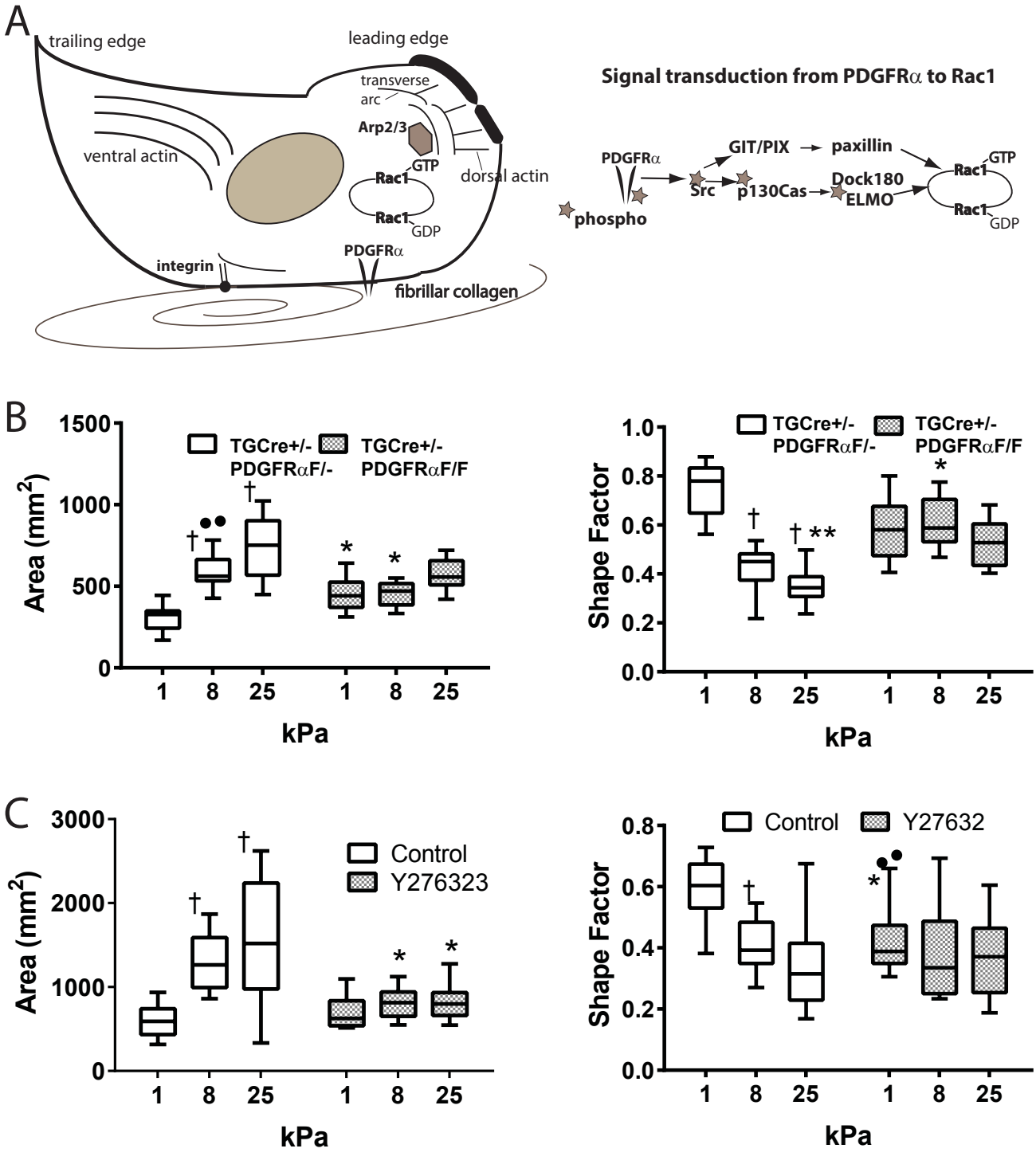
A
trailing edge
leading edge
transverse arc
Arp2/3
ventral actin
GTP
Rac1
dorsal actin
Rac1
GDP
PDGFRα
integrin
fibrillar collagen
Signal transduction from PDGFRα to Rac1
PDGFRα
GIT/PIX
paxillin
Src
p130Cas
Dock180
ELMO
Rac1
GTP
Rac1
GDP
phospho
B
Area (mm2)
TGCre+/- PDGFRαF/-
TGCre+/- PDGFRαF/F
kPa
Shape Factor
C
Control
Y276323
Y27632

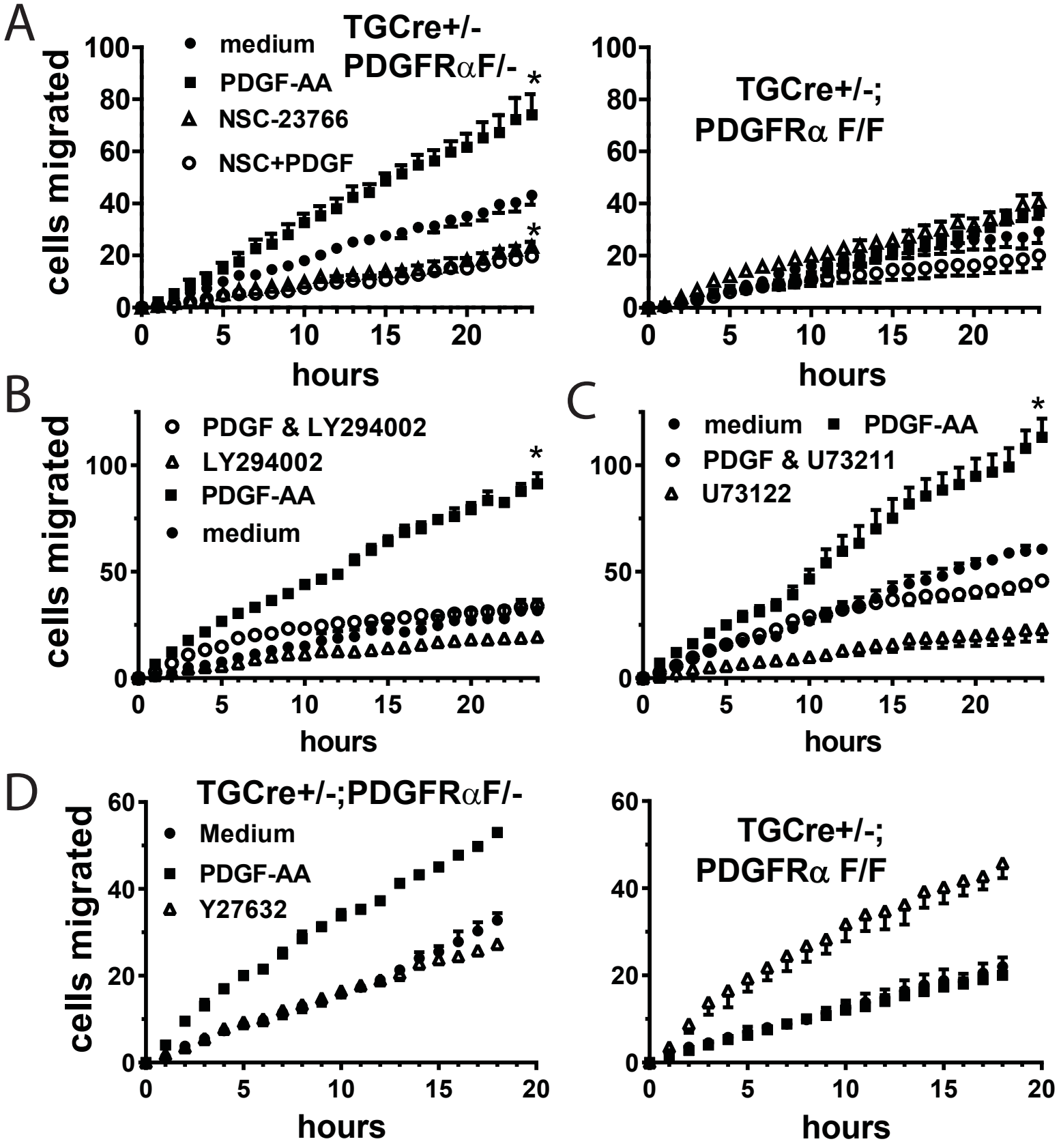
A
TGCre+/-
PDGFRαF/-
medium
PDGF-AA
NSC-23766
NSC+PDGF
cells migrated
hours
TGCre+/-;
PDGFRα F/F
B
PDGF & LY294002
LY294002
PDGF-AA
medium
C
medium
PDGF-AA
PDGF & U73211
U73122
D
TGCre+/-;PDGFRαF/-
Medium
PDGF-AA
Y27632

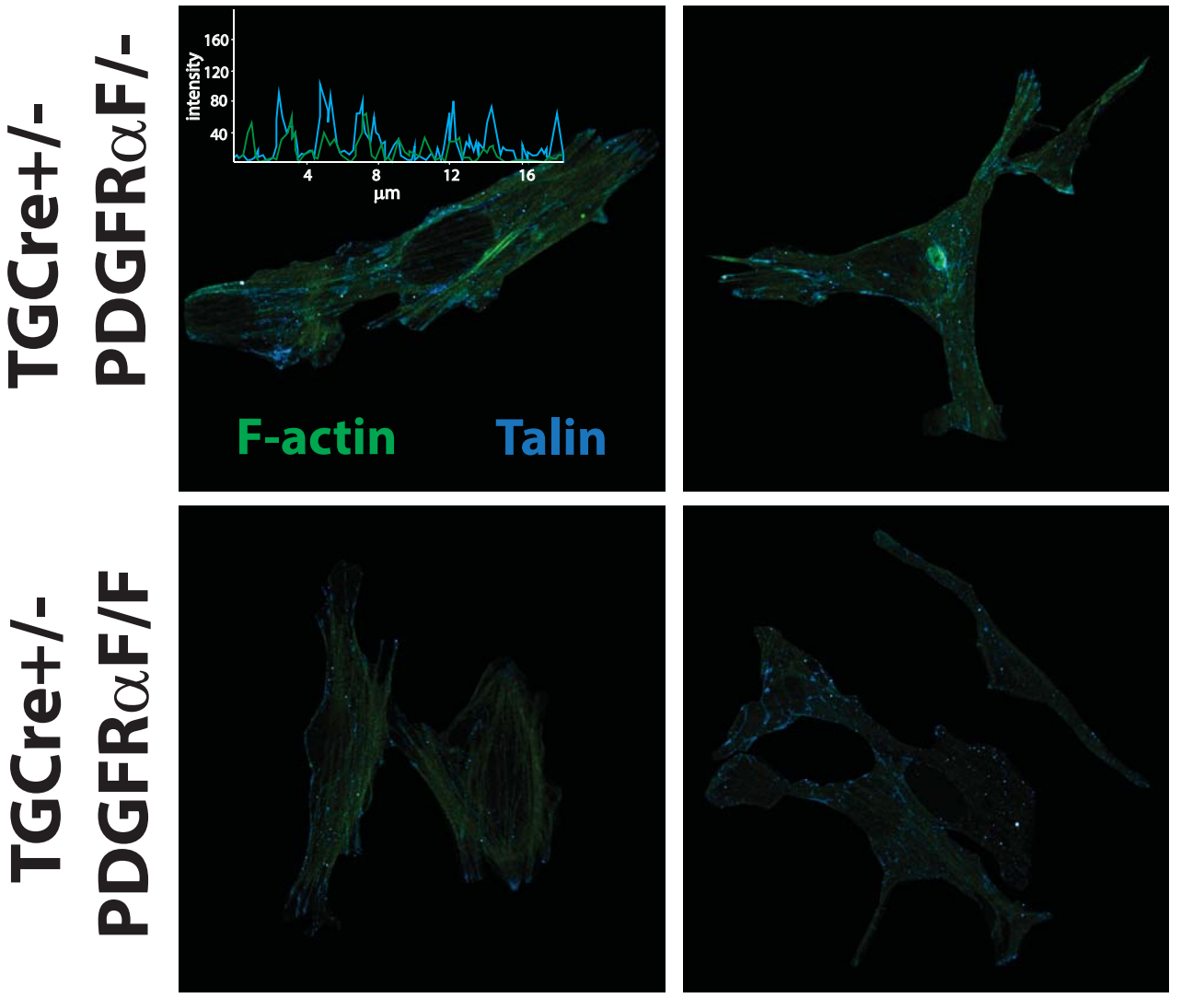
A
medium
Y27632
TGCre+/-
PDGFRαF/-
TGCre+/-
PDGFRαF/F
intensity
160
120
80
40
4
8
12
16
µm
F-actin
Talin

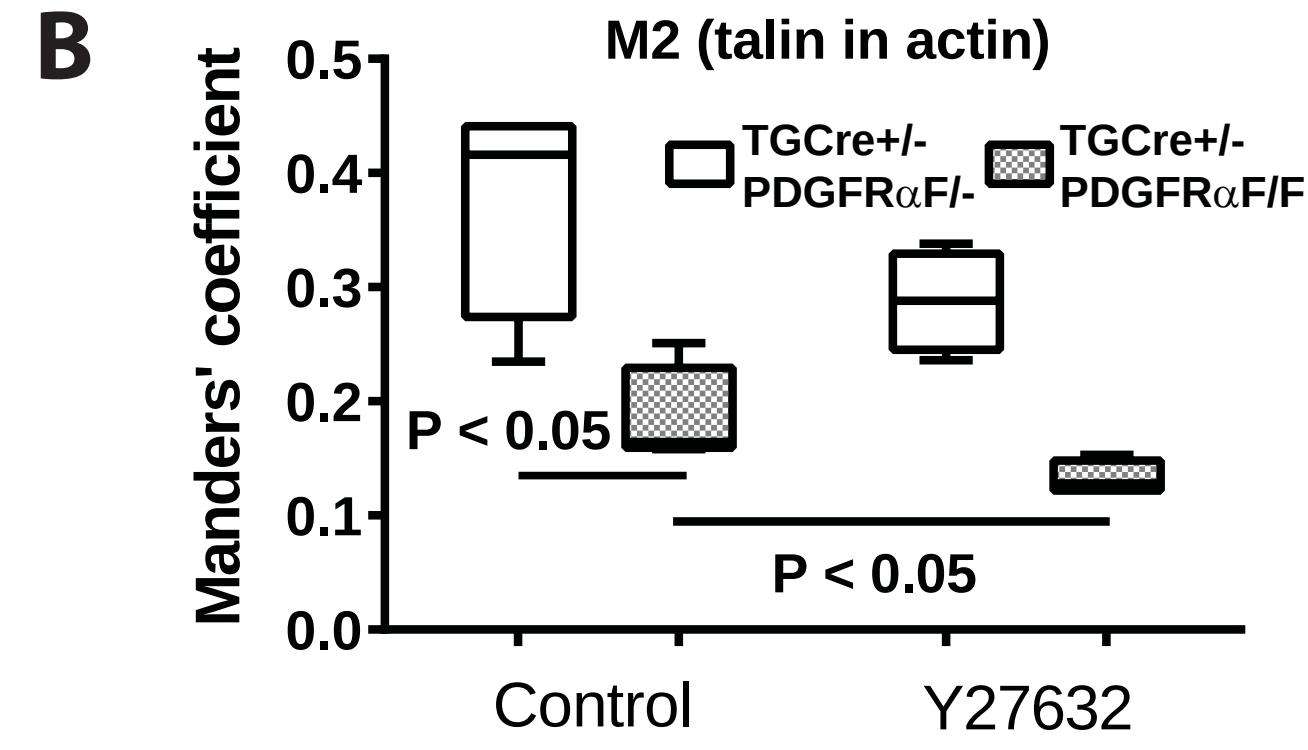
B
M2 (talin in actin)
Manders' coefficient
0.5
0.4
0.3
0.2
0.1
0.0
TGCre+/-
PDGFRαF/-
TGCre+/-
PDGFRαF/F
P < 0.05
P < 0.05
Control
Y27632

A

medium

NSC23766

TGCre+/-;PDGFRαF/-

F-actin Talin pPaxillin

TGCre+/1;PDGFRαF/F

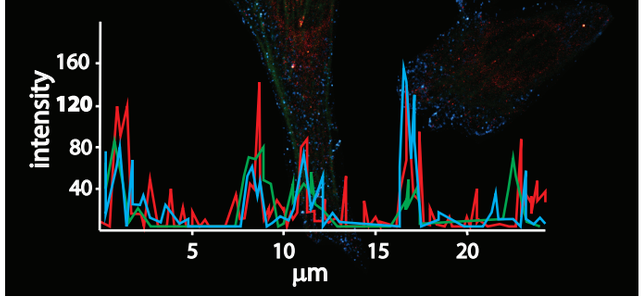

B

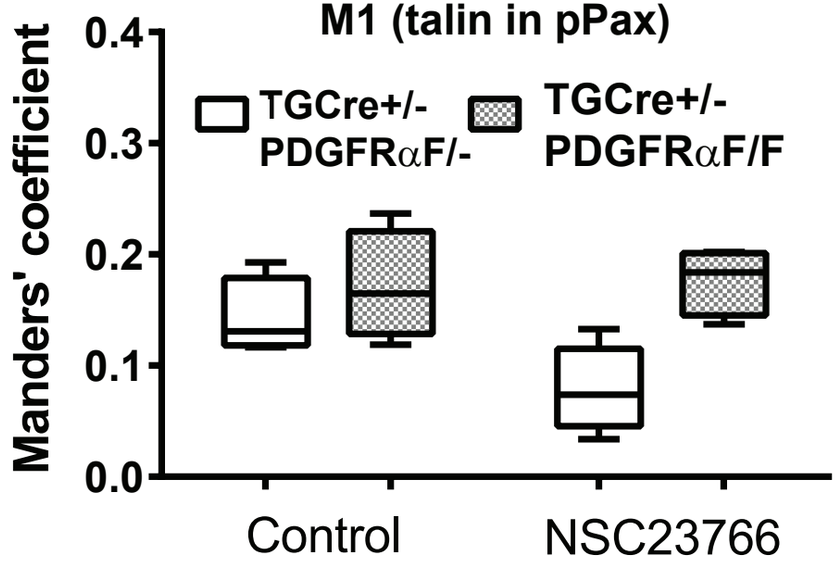

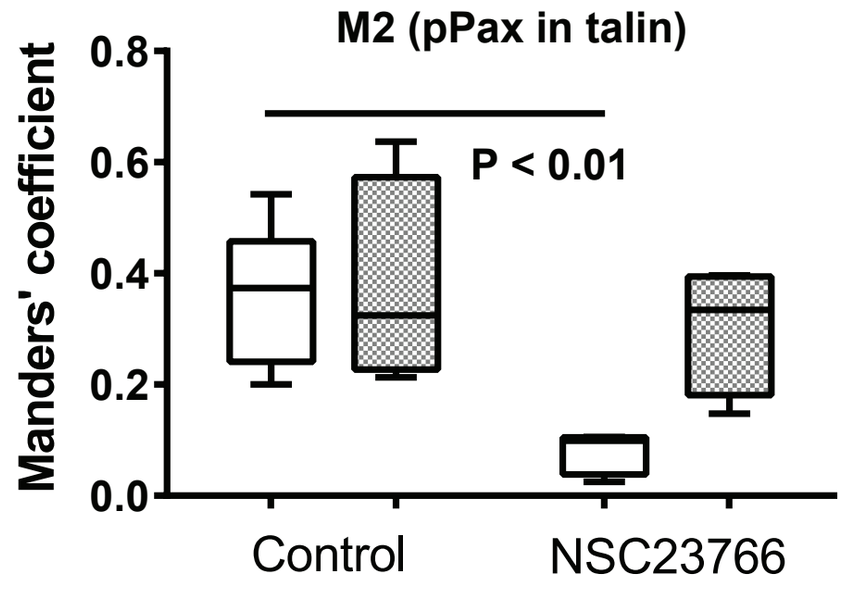

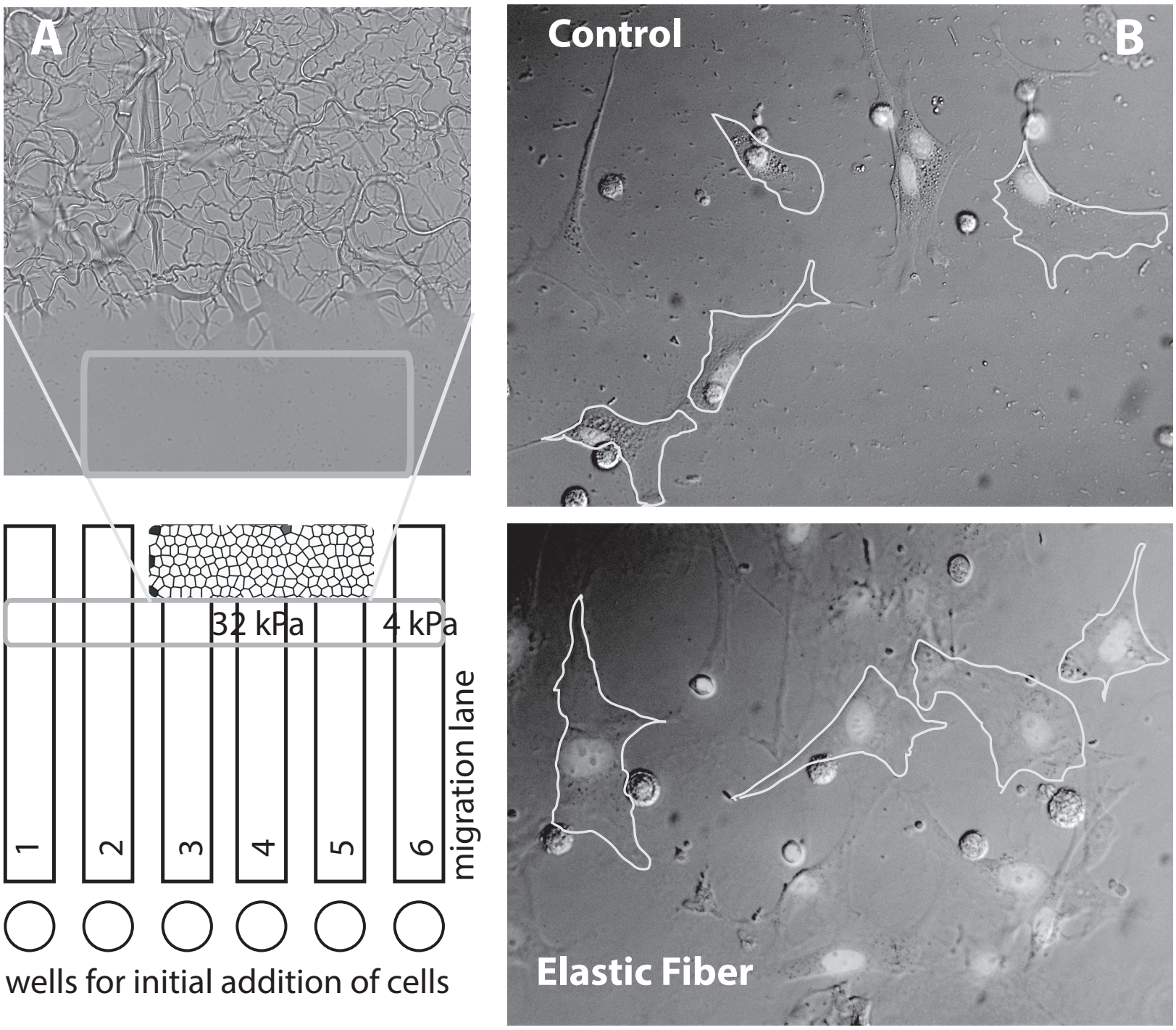
A
Control
B
32 kPa
4 kPa
1
2
3
4
5
6
migration lane
wells for initial addition of cells
Elastic Fiber

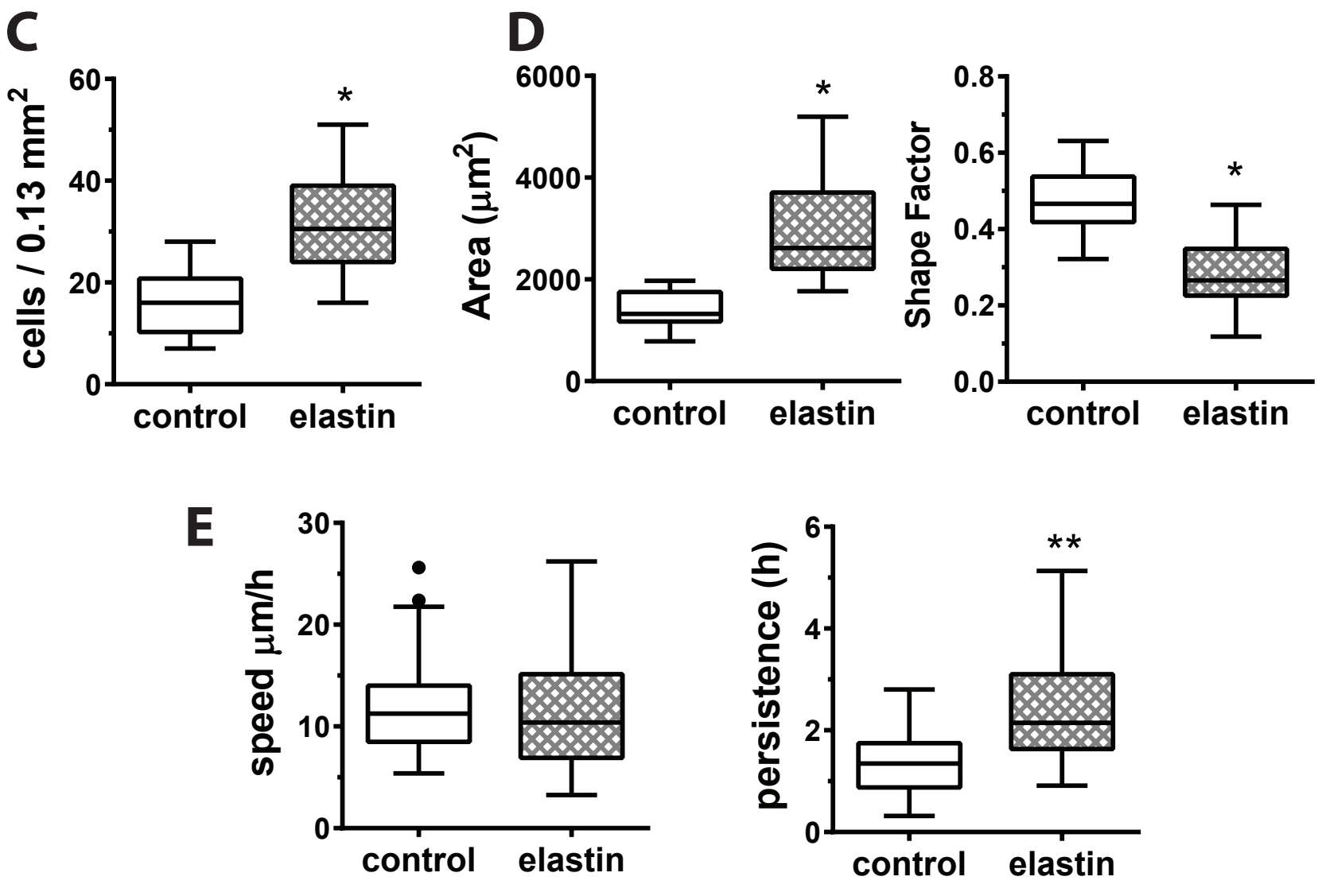
C
cells / 0.13 mm2
60
40
20
0
*
control
elastin
D
Area (µm2)
6000
4000
2000
0
*
control
elastin
Shape Factor
0.8
0.6
0.4
0.2
0.0
*
control
elastin
E
speed µm/h
30
20
10
0
control
elastin
persistence (h)
6
4
2
0
**
control
elastin

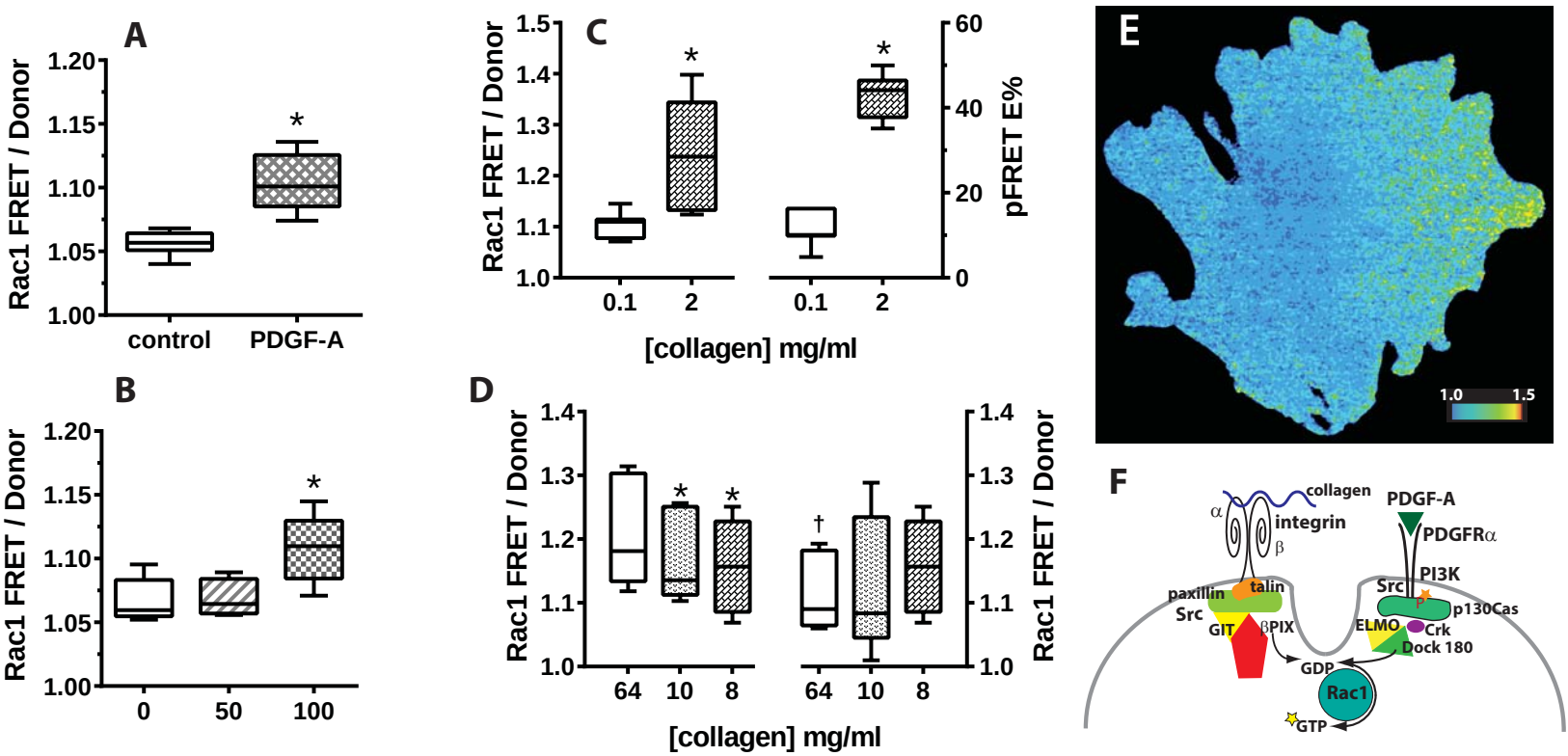
A
Rac1 FRET / Donor
1.20
1.15
1.10
1.05
1.00
*
control
PDGF-A
B
Rac1 FRET / Donor
1.20
1.15
1.10
1.05
1.00
*
0
50
100
C
Rac1 FRET / Donor
1.5
1.4
1.3
1.2
1.1
1.0
*
*
pFRET E%
60
40
20
0
0.1
2
0.1
2
[collagen] mg/ml
D
Rac1 FRET / Donor
1.4
1.3
1.2
1.1
1.0
*
*
†
64
10
8
64
10
8
Rac1 FRET / Donor
[collagen] mg/ml
E
1.0
1.5
F
collagen
α
integrin
β
PDGF-A
PDGFRα
PI3K
Src
p
p130Cas
paxillin
talin
Src
GIT
βPIX
ELMO
Crk
Dock 180
GDP
Rac1
GTP

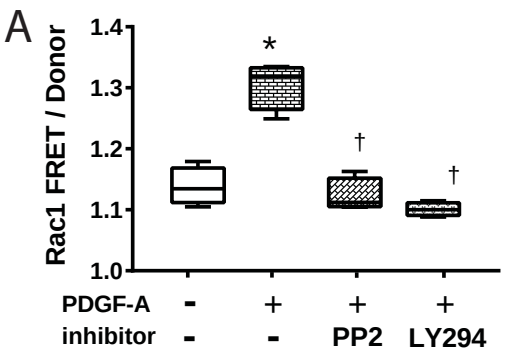
A
Rac1 FRET / Donor
1.4
1.3
1.2
1.1
1.0
*
†
†
PDGF-A - + + +
inhibitor - - PP2 LY294

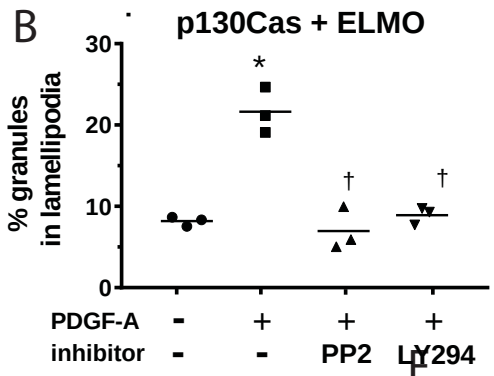
B
p130Cas + ELMO
% granules in lamellipodia
30
20
10
0
*
†
†
PDGF-A - + + +
inhibitor - - PP2 LY294

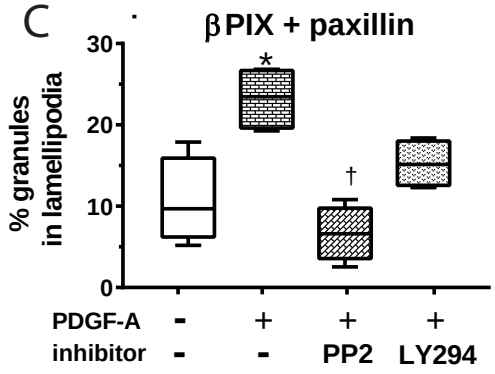
C
βPIX + paxillin
% granules in lamellipodia
30
20
10
0
*
†
PDGF-A - + + +
inhibitor - - PP2 LY294

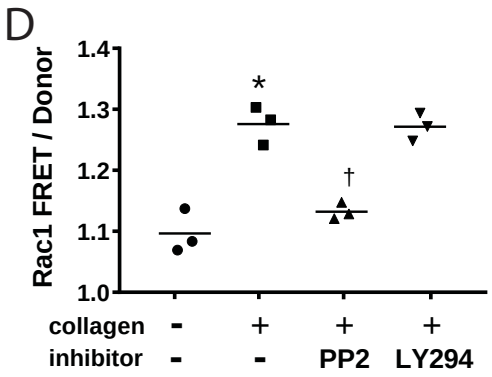
D
Rac1 FRET / Donor
1.4
1.3
1.2
1.1
1.0
*
†
collagen - + + +
inhibitor - - PP2 LY294

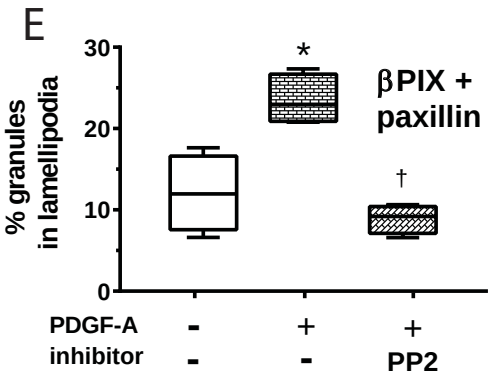
E
% granules in lamellipodia
30
20
10
0
*
βPIX + paxillin
†
PDGF-A - + +
inhibitor - - PP2

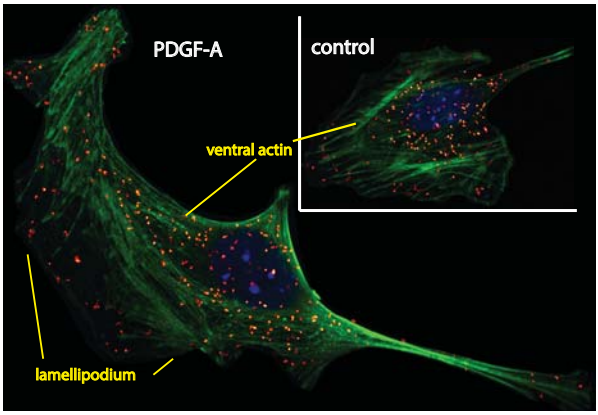
F
PDGF-A
control
ventral actin
lamellipodium